Imperial College
London

MPhil to PhD Transfer Report

Single and Multichannel Sampling of Signals with Finite Rate of Innovation Using E-Splines

December 2008

Author: Hojjat Akhondi Asl

Supervisor: Dr. P.L. Dragotti

Abstract

Exponential splines (E-splines), finite support splines that can reproduce real or complex exponentials, can be used as sampling kernels to sample 1-D signals with finite rate of innovation (FRI). Furthermore, unlike polynomial reproducing kernels, E-splines kernels can be used to sample 1-D FRI signals in a truly symmetric, multichannel sampling scenario where the sampling process is separated between the different sensors. However, E-splines have not been considered in single and multichannel sampling of multidimensional FRI signals.We present our novel sampling algorithms for single and multichannel sampling of stream of 2-D Diracs and bilevel polygons using E-splines. For the multichannel sampling case, we consider a bank of E-spline filters to acquire a 2-D signal, where each filter has access to a delayed version of the input signal. It will be shown that, by registering the delay parameters from the relevant features of the signal samples, it is possible to synchronize the different channels exactly so that perfect reconstruction of the original signal and its delayed versions is achieved.

Contents

1 Introduction **3**

1.1 Background, Problem Statement and Related Work 3

1.2 Original Contribution 4

1.3 Organization of the Report 4

2 Sampling Frameworks for Signals with Finite Rate of Innovation **5**

2.1 Introduction 5

2.2 Sampling Setup 5

2.2.1 Definition of 1-D Signals with Finite Rate of Innovation 6

2.2.2 Sampling Kernels 6

2.2.3 Reconstruction Algorithms 8

2.3 Multidimensional Sampling Framework 13

3 Sampling Multidimensional FRI Signals Using E-Splines **16**

3.1 Introduction 16

3.2 Sampling and Reconstructing 2-D Diracs Using E-splines 16

3.2.1 ACMP Method 18

3.2.2 A Sampling Theorem For Reconstructing 2-D Diracs Using E-Splines 22

3.3 Sampling and Reconstructing Bilevel Polygons Using E-splines 22

3.3.1 Fourier Transform of a Polygonal Shape Function 22

3.3.2 Introduction to Radon Transform 24

3.3.3 Projection-Slice Theorem 25

3.3.4 A Sampling Theorem For Reconstructing Bilevel Polygons Using E-Splines 26

4 Multichannel Sampling of FRI Signals with E-Splines **32**

4.1 Introduction 32

4.2 Multichannel Sampling of 1-D Diracs 33

4.3 Multichannel Sampling of Multidimensional FRI Signals 34

5 Future Research **40**

5.1 Sampling Bilevel Polygons 40

5.2 Sampling Under Noisy Conditions 40

5.3 Multichannel Sampling of Bilevel Polygons 40
5.4 Applications 41

Chapter 1

Introduction

1.1 Background, Problem Statement and Related Work

Sampling theory plays a fundamental role in modern signal processing and communications. In 1949 Shannon published the famous sampling theorem that states, any bandlimited signal can be sampled and perfectly reconstructed if the sampling rate is chosen at a rate equal to or greater than twice the maximum bandwidth of the signal. This theorem is mostly known as Shannon's sampling theorem and was published by Shannon in 1949 in his famous paper "Communication in the presence of noise". One of the drawbacks of this theorem is that the input signal must be bandlimited and real world signals are never exactly bandlimited. Recently, it was shown [1, 2] that it is possible to sample and perfectly reconstruct some classes of non-bandlimited signals. Signals that can be reconstructed using this framework are called signals with Finite Rate of Innovation (FRI) as they can be completely defined by a finite number of parameters. Stream of weighted Diracs and piecewise polynomial signals are some examples of FRI signals.

The results of [1, 2] apply to one dimensional FRI signals only. More recently, the extensions to the multidimensional case were considered by Maravic [20] and Shukla [13] where, Maravic et al. [20] considered sampling theorems for some 2-D FRI signals, such as 2-D stream of Diracs and bilevel polygons using the Sinc and Gaussian sampling kernels, while Shukla et al. [13] proposed algorithms, from the theory of complex moments, for sampling 2-D stream of Diracs and bilevel polygons with the use of B-splines as the sampling kernel (a polynomial reproducing kernel).

Dragotti et al. [2] showed that, exponential splines [3] (E-splines), another important family of kernels, can be used as the sampling kernel to sample 1-D FRI signals. Moreover, Baboulaz [11] showed in his paper that, unlike the polynomial reproducing kernels, exponential spline sampling kernels can be employed in a fully symmetric multichannel sampling environment. In [11] it is shown that, with the use of E-splines, it is possible to sample and perfectly reconstruct one dimensional FRI signals (1-D Diracs) in a fully symmetric, noiseless, multichannel sampling environment. Thus far, exponential splines, splines that can reproduce real or complex exponentials, have not been considered in sampling

multidimensional signals. Moreover, E-splines have not been considered in the scenario of symmetric, multichannel sampling of multidimensional FRI signal.

In our research work, our first objective is to extend the use of E-splines to the sampling of multidimensional FRI signals. Then we want to investigate the use of E-spline sampling kernels for the case of multichannel sampling of multidimensional FRI signals. Multichannel sampling framework is used in many modern applications such as image super-resolution in multi-camera systems [23, 24, 25] and in interleaved A/D converters and we want to see if E-splines, as the sampling kernels, have the potential to be used in such contexts. Our research work is mainly concerned with investigating the advantages and capabilities of exponential splines over the current methods used for single and multichannel sampling of multidimensional FRI signals.

1.2 Original Contribution

Over the last year, our contribution to the field of sampling multidimensional FRI signals with the use of E-spline sampling kernels, led to the submission of a paper with the title "A Sampling Theorem For Bilevel Polygons Using E-Splines", which is going to appear on the "8th IMA Conference on Mathematics in Signal Processing".

1.3 Organization of the Report

The outline of the report is as follows: In Chapter II, we will look at some preliminaries and background needed for sampling signals with finite rate of innovation, where we go through the sampling setup, different classes of finite support kernels, and also a general overview on the reconstruction algorithms. In Chapter III, we present our novel sampling theorems for the reconstruction of 2-D Diracs and also bilevel polygons using exponential splines. In Chapter IV we present our novel sampling theorems for the reconstruction of 2-D Diracs and bilevel polygons in a symmetric multichannel scenario using exponential splines as the sampling kernels. A discussion on the problems we have had and also a future research plan over the next coming year will be discussed in Chapter V. In the Appendix, it is shown how a modified version of the ACMP method (a method used for retrieving unknown parameters such as phase, amplitude and frequency from the frequency content of a signal; detailed description of the method is explained in Chapter III) can be used for information retrieval, such as amplitude and frequency, from different data models other than the standard data model used for harmonic data retrieval methods.

Chapter 2

Sampling Frameworks for Signals with Finite Rate of Innovation

2.1 Introduction

We all know that bandlimited signals can be sampled and reconstructed perfectly with Shannon's famous sampling theorem. As mentioned in the previous chapter, recently Vetterli et al. [1] showed that it is possible to sample and perfectly reconstruct non-bandlimited signals with FRI, such as stream of Diracs, nonuniform splines and piecewise polynomials. The reconstruction of 1-D FRI signals is based on the annihilating filter method (also known as Prony's method), a tool widely used in spectral estimation [18] and error-correction coding [19]. The sampling kernels considered in [1], that is the sinc and the Gaussian kernels, have an infinite support and are therefore not physically realizable. Moreover, the use of such kernels make the reconstruction algorithm complex and unstable. Dragotti et al. [2] showed that many 1-D FRI signals with local finite rate of innovation can be sampled and reconstructed using a wide range of sampling kernels that have finite support. Such kernels have the property of reproducing polynomials or exponentials and deliver practical implementation of the same sampling and retrieval techniques used in [1] for 1-D FRI signals. In the next section we will go through the sampling setup used for 1-D FRI signals, the definition of 1-D FRI signals, different classes of finite support sampling kernels and two examples for the reconstruction algorithms, the annihilating filter method [1, 2] and the standard subspace harmonic retrieval method [18].

2.2 Sampling Setup

Figure 2.1 shows the sampling setup for 1-D FRI signals where $g(x)$ represents the input 1-D FRI signal, $h(x)$ the impulse response of the acquisition device, $\phi(x)$ a rescaled and time-reversed version of $h(x)$ (also known as the sampling kernel), $g_s(x)$ the sampled version of the input signal $g(x)$, s_k the samples and T is the sampling interval. The box C/D (continuous-to-discrete) reads out the sample values s_k from $g_s(x)$. Using the setup

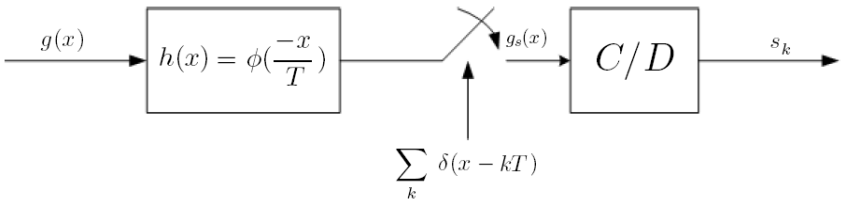

Figure 2.1: **1-D FRI sampling setup**

shown in Figure 2.1, the samples s_k are given by:

$$s_k = g(x) * h(x)|_{x=kT} \tag{2.1}$$

$$= \int_{-\infty}^{\infty} g(x)\ \phi(\frac{x}{T} - k)\ dx \tag{2.2}$$

$$= \langle g(x), \phi(\frac{x}{T} - k)\rangle. \tag{2.3}$$

We want to see under what conditions we can achieve perfect reconstruction of $g(x)$ from the samples s_k. We thus need to define FRI signals, introduce the sampling kernels used and discuss the reconstruction procedures.

2.2.1 Definition of 1-D Signals with Finite Rate of Innovation

Let us consider a 1-D signal of the form [2]:

$$g(x) = \sum_{r=0}^{N} \sum_{j \in \mathbb{Z}} \gamma_{j,r}\ \phi_r(x - x_j). \tag{2.4}$$

The degrees of freedom of the signal $g(x)$ are the shifts x_j and the coefficients $\gamma_{j,r}$, assuming that the set of functions $\phi_r(x)$ are known. If we introduce a counting function $C_g(x_a, x_b)$ which counts the number of free parameters of $g(x)$ over the interval $\tau = [x_a, x_b]$, then the rate of innovation ρ of the signal $g(x)$ is defined as:

$$\rho = \lim_{\tau \to \infty} \frac{1}{\tau}\ C_g(-\tau/2, \tau/2). \tag{2.5}$$

If ρ is finite, then the signal is said to have a finite rate of innovation. It is important to note that all shift-invariant signals, including bandlimited signals could be defined with the above definition. The rate of innovation of real-valued bandlimited signals is: $\rho = 2 \times f_{max}$ where f_{max} is the maximum frequency of the bandlimited signal.

2.2.2 Sampling Kernels

Sampling kernels are characterized by the physical properties of the acquisition device which are normally specified and cannot be modified. Unlike the classical sampling schemes, FRI sampling schemes provide a larger choice of kernels that allow perfect reconstruction

of the input signal. In [2] different classes of finite support kernels are defined. Here, we explain the two most important ones, polynomial and exponential reproducing kernels (For simplicity assume $T = 1$ when not specified).

Polynomial Reproducing Kernels

Any kernel $\phi(x)$ that together with its shifted versions can reproduce polynomials of maximum degree M is called a polynomial reproducing kernel. That is any kernel satisfying the following property:

$$\sum_{n\in\mathbb{Z}} c_n^m \phi(x-n) = x^m, \tag{2.6}$$

for a proper choice of coefficients c_n^m with $m = 0, 1, \ldots, M$. Note that the subscript n represents the shifts index and the superscript m represents the polynomial degree. The choice of M depends on the local rate of innovation of the signal $g(x)$ and will be discussed later on. Polynomial reproducing kernels include any function satisfying the so-called Strang-Fix conditions [34] which states that the kernel $\phi(x)$ satisfies equation (2.6) if and only if its Fourier transform $\hat{\phi}(\omega)$ satisfies:

$$\hat{\phi}(0) \neq 0 \text{ and } \hat{\phi}^{(m)}(2n\pi) = 0 \text{ for } n \neq 0 \text{ and } m = 0, 1, \ldots, M, \tag{2.7}$$

where the superscript (m) stands for the m-th derivative of $\hat{\phi}(\omega)$. B-splines [29, 30, 31] and Daubechies scaling functions [32, 33] are examples of kernels satisfying the Strang-Fix conditions. Furthermore, the coefficients c_n^m are given by:

$$c_n^m = \int_{-\infty}^{\infty} x^m \tilde{\phi}(x-n)\, dx, \tag{2.8}$$

where $\tilde{\phi}(x)$ is chosen to form a dual basis [12] of $\phi(x)$, that is $\langle \tilde{\phi}(x-j), \phi(x-k) \rangle = \delta_{j,k}$. Since Daubechies scaling functions are orthogonal functions, then: $\tilde{\phi}(x) = \phi(x)$. B-splines are biorthogonal functions and their dual basis is defined in [35].

Exponential Reproducing Kernels

Any kernel $\phi(x)$ that together with its shifted versions can reproduce real or complex exponentials in the form $e^{\alpha_m x}$ with $\alpha_m = \alpha_0 + m\lambda$ and $m = 0, 1, \ldots, M$ is called an exponential reproducing kernel. That is any kernel satisfying the following property:

$$\sum_{n\in\mathbb{Z}} c_n^m \phi(x-n) = e^{\alpha_m x}, \tag{2.9}$$

for a proper choice of coefficients c_n^m.

The theory of exponential reproducing kernels is quite recent and is based on the notion

of exponential splines (E-splines) [3]. A function $\hat{\beta}_{\vec{\alpha}}(x)$ with Fourier transform

$$\hat{\beta}_{\vec{\alpha}}(\omega) = \prod_{m=0}^{M} \frac{1 - e^{\alpha_m - j\omega}}{j\omega - \alpha_m}, \tag{2.10}$$

is called E-spline of order M where $\vec{\alpha} = (\alpha_0, \alpha_1, \ldots, \alpha_M)$. The produced spline has compact support and can reproduce any exponential in the subspace spanned by $(e^{\alpha_0 x}, e^{\alpha_1 x}, \ldots, e^{\alpha_M x})$. Moreover, the values of α_0 and λ can be chosen arbitrarily, but too small or too large values could lead to unstable results for the reproduction of exponentials. E-splines are biorthogonal functions and the coefficients c_n^m can be found using the dual of $\hat{\beta}_{\vec{\alpha}}(x)$.

2.2.3 Reconstruction Algorithms

For most one dimensional FRI signals, the problem of reconstructing $g(x)$ is reduced to the problem of reconstructing a set of 1-D Diracs. For example, in [1], it is shown that the problem of reconstructing non-uniform splines can be reduced to the problem of reconstructing stream of 1-D Diracs. Also, in the case of piecewise polynomials, the reconstruction procedure is reduced to reconstructing a sum of derivatives of Diracs. For this reason we concentrate on stream of Diracs only. Let us assume our input signal $g(x)$ consists of K Diracs, that is:

$$g(x) = \sum_{k=1}^{K} a_k \delta(x - x_k). \tag{2.11}$$

The signal is sampled using the sampling setup shown in Figure 2.1 with a sampling kernel $\phi(x)$. Therefore, as previously stated, the samples s_k are given as: $s_k = \langle g(x), \phi(x - k) \rangle$. In [2], it is shown that such representation of stream of Diracs can be perfectly reconstructed using polynomial or exponential reproducing kernels. Let us consider the following weighted sum of the samples:

$$\tau_m = \sum_k c_k^m s_k. \tag{2.12}$$

Substituting the equation for the samples $s_{j,k}$ into the above equation, gives us:

$$\tau_m = \langle g(x), \sum_k c_k^m \phi(x - k) \rangle. \tag{2.13}$$

The second term in the inner product can be replaced by one of the equations defined in (2.6) or (2.9) depending on what kernel is being used as the sampling kernel. If polynomial reproducing kernels are used, then from equation (2.13), the polynomial (or geometric) moments of the signal are obtained:

$$\tau_m = \int_{-\infty}^{\infty} g(x)\, x^m\, dx, \tag{2.14}$$

and assuming that our input signal is a set of K 1-D Diracs, we have:

$$\tau_m = \sum_{k=0}^{K-1} a_k \, x_k^m, \qquad m = 0, 1, \ldots, M \tag{2.15}$$

Likewise, for exponential reproducing kernels, the exponential moments of the signal are obtained, that is:

$$\tau_m = \int_{-\infty}^{\infty} g(x) \, e^{\alpha_m x} \, dx \tag{2.16}$$

$$= \sum_{k=0}^{K-1} a_k \, e^{\alpha_m x_k}, \qquad m = 0, 1, \ldots, M \tag{2.17}$$

$$= \sum_{k=0}^{K-1} \tilde{a_k} \, u_k^m, \qquad \text{where } \tilde{a_k} = a_k e^{\alpha_0 x_k} \text{ and } u_k = e^{\lambda x_k}. \tag{2.18}$$

Therefore for both cases the given expressions can be expressed as a power-sum series in the form:

$$\tau_m = \sum_{k=0}^{K} a_k \, u_k^m, \quad m = 1, 2, \ldots, M. \tag{2.19}$$

In 1795 Prony showed that the unknown parameters a_k and u_k can be exactly recovered, provided that the number of measurements of τ_m is at least $2K$. Subspace harmonic retrieval methods could also be used to recover the amplitudes and the locations of the Diracs from the measurements τ_m. Both methods, that is the annihilating filter method and the matrix pencil method (a subspace harmonic retrieval method) will be explained in the next section.

Annihilating Filter Method

Let us define a filter h_m with $m = 0, 1, \ldots, K$, such that the locations u_k are the roots of the filter. The z-transform of such a filter is:

$$H(z) = \sum_{m=0}^{K} h_m z^{-m} = \prod_{k=0}^{K-1} (1 - u_k z^{-1}). \tag{2.20}$$

The observed signal τ_m convolved with the filter defined above, results in:

$$\begin{aligned} h_m * \tau_m &= \sum_{i=0}^{K} h_i \, \tau_{m-i} \\ &= \sum_{i=0}^{K} \sum_{k=0}^{K-1} a_k \, h_i \, u_k^{m-i} \\ &= \sum_{k=0}^{K-1} a_k \, u_k^m \underbrace{\sum_{i=0}^{K} h_i \, u_k^{-i}}_{=0}, \end{aligned}$$

The under-braced term in the set of equations above equals to zero, as $H(u_k) = 0$, thus:

$$h_m * \tau_m = 0. \tag{2.21}$$

The filter $H(z)$ is called the annihilating filter as it annihilates the observed signal τ_m. The zeros of such a filter uniquely define the distinct locations u_k. Moreover, the convolution equation can be written in the matrix form as follows:

$$\begin{bmatrix} \tau_K & \tau_{K-1} & \cdots & \tau_0 \\ \tau_{K+1} & \tau_K & \cdots & \tau_1 \\ \vdots & \vdots & \ddots & \vdots \\ \tau_N & \tau_{N-1} & \cdots & \tau_{N-K} \end{bmatrix} \times \begin{bmatrix} h(0) \\ h(1) \\ \vdots \\ h(K) \end{bmatrix} = 0,$$

where $N \geq 2K - 1$ as at least $2K$ consecutive values of τ_m are required in order to solve the matrix equation shown above. The above expression indicates that the matrix is rank deficient, but since $h(0) = 1$, it can be written as a system of Yule-Walker equations:

$$\begin{bmatrix} \tau_{K-1} & \tau_{K-2} & \cdots & \tau_0 \\ \tau_K & \tau_{K-1} & \cdots & \tau_1 \\ \vdots & \vdots & \ddots & \vdots \\ \tau_{N-1} & \tau_{N-2} & \cdots & \tau_{N-K} \end{bmatrix} \times \begin{bmatrix} h(1) \\ h(2) \\ \vdots \\ h(K) \end{bmatrix} = - \begin{bmatrix} \tau_K \\ \tau_{K+1} \\ \vdots \\ \tau_N \end{bmatrix},$$

where by taking the inverse of the first matrix we can solve for the coefficients h_m. Given the filter coefficients, the locations of the Diracs are found by taking the roots of the filter. The system of equations above gives a unique solution for u_k since the filter coefficients h_m are unique for a given signal (if there are multiple poles, for example $u_{k-1} = u_k$, then the most-left matrix above will be rank deficient and the filter coefficients h_m will not be unique). After finding the locations u_k, we are able to find the weights a_k from the power-series formula given in equation (2.19). By expanding the equation and writing it

in the matrix form, we obtain:

$$\begin{bmatrix} 1 & 1 & \cdots & 1 \\ u_0 & u_1 & \cdots & u_{K-1} \\ u_0^2 & u_1^2 & \cdots & u_{K-1}^2 \\ \vdots & \vdots & \ddots & \vdots \\ u_0^{K-1} & u_1^{K-1} & \cdots & u_{K-1}^{K-1} \end{bmatrix} \times \begin{bmatrix} \alpha_0 \\ \alpha_1 \\ \vdots \\ \alpha_{K-1} \end{bmatrix} = \begin{bmatrix} \tau_0 \\ \tau_1 \\ \vdots \\ \tau_{K-1} \end{bmatrix}.$$

The above system of equations is a Vandermonde system and leads to a unique solution for the amplitudes a_k since the u_k are distinct.

Matrix Pencil Method

The field of harmonic retrieval problem, which is related to estimating frequency contents of a signal, has a vast range of applications in signal processing. Although there are many harmonic retrieval methods available, most of them suffer from resolution inaccuracy and large amount of computational burden. Subspace harmonic retrieval methods are generally more efficient than the classical methods [18, 39, 40]. The well-known methods such as ESPRIT [37] (Estimation of Signal Parameters via Rotational Invariance Techniques) and MUSIC [38] (MULtiple Signal Classification) are examples of subspace harmonic retrieval methods for one dimensional signals where matrix decomposition techniques are used to estimate unknown parameters such as amplitude, phase and frequency. In this section we will explain the standard 1-D subspace harmonic retrieval method, the matrix pencil method, which makes the use of Hankel matrices, singular-value-decomposition and Eigen-value-decomposition.

Like before, let us consider that we have access to the measurements τ_m, which consists of a sum of K polynomials or exponentials (real or complex) with unknown locations u_k and amplitude a_k. Then we arrange the data points into a Hankel matrix H of dimension $L \times M$ as follows:

$$H_{L\times M} = \begin{bmatrix} \tau_0 & \tau_1 & \cdots & \tau_{M-1} \\ \tau_1 & \tau_2 & \cdots & \tau_M \\ \vdots & \vdots & \ddots & \vdots \\ \tau_{L-1} & \tau_{L-2} & \cdots & \tau_{N-1} \end{bmatrix},$$

where $L \geq K+1$, $M \geq K$ and $N \geq 2K-1$, therefore, as for the annihilating filter method, the number of measurements of τ_m should be at least $2K$. The matrix H, with the arrangement shown, is a product of three matrices: S, A and T where S and T are Vandermonde matrices of the poles u_k and A is a diagonal matrix containing the amplitudes a_k. More precisely, the Hankel matrix H can be written as:

$$H = SAT^T, \tag{2.22}$$

with the decomposition illustrated as follows:

$$H = \begin{bmatrix} 1 & 1 & \dots & 1 \\ u_1 & u_2 & \dots & u_K \\ \vdots & \vdots & \ddots & \vdots \\ u_1^{L-1} & u_2^{L-1} & \dots & u_K^{L-1} \end{bmatrix} \begin{bmatrix} a_1 & 0 & \dots & 0 \\ 0 & a_2 & \dots & 0 \\ \vdots & \vdots & \ddots & \vdots \\ 0 & 0 & \dots & a_K \end{bmatrix} \begin{bmatrix} 1 & 1 & \dots & 1 \\ u_1 & u_2 & \dots & u_K \\ \vdots & \vdots & \ddots & \vdots \\ u^{M-1} & u_2^{M-1} & \dots & u_K^{M-1} \end{bmatrix}^T .$$

The Singular-Value-Decomposition (SVD) decomposes a matrix into a product of three matrices: U, Σ and V where $U^H.U = I$, $V^H.V = I$ and Σ is a diagonal matrix containing the singular values. Here, the superscript H stands for the Hermitian transpose. If we take the SVD of the described Hankel matrix H, we obtain:

$$H_{L\times M} = U_{L\times L}\Sigma_{L\times M}V^H_{M\times M}. \tag{2.23}$$

In order to obtain the signal subspace, only the product of the first K columns of the matrices U and V, and also the $K \times K$ upper left matrix of Σ are taken into account, that is:

$$H = [U_K \dots] \begin{bmatrix} \Sigma_K & \cdots \\ \cdots & \cdots \end{bmatrix} [V_K \dots]^H \;\Rightarrow\; U_K\Sigma_K V_K^H.$$

Thus, the resulting matrix is a truncated version of the original matrix H:

$$H_K = U_K\Sigma_K V_K^H. \tag{2.24}$$

Since the matrices S and U_K span the same column space, the following important relationship holds true:

$$U_K = S.Q, \tag{2.25}$$

where Q is a non-singular matrix of dimension $K \times K$. We mentioned that the matrices S and T have a Vandermonde structure. Vandermonde matrices satisfy the "shift-invariant" subspace property which states that if $\overline{\boldsymbol{S}}$ and $\underline{\boldsymbol{S}}$ denote the matrix S after omission of the first and the last row respectively then the following relationship is valid:

$$\overline{S} = \underline{S}.\Phi, \tag{2.26}$$

where $\Phi = diag\{u_1, u_2, \dots, u_K\}$. Knowing that $U_K = S.Q$, we clearly have (true for any matrix multiplication):

$$\underline{U_K} = \underline{S}.Q \tag{2.27}$$

$$\overline{U_K} = \overline{S}.Q \tag{2.28}$$

$$= \underline{S}.\Phi.Q. \tag{2.29}$$

Now let us consider the matrix pencil $(\overline{U_K}, \underline{U_K})$ as follows:

$$\overline{U_K} - \lambda \underline{U_K} = \underline{S}(\Phi - \lambda I)Q, \tag{2.30}$$

where λ is called the rank reducing number. We can solve for Φs by finding the Eigen-values of the matrix pencil. The problem of finding the Eigen-values of a matrix pencil is called the "Generalized Eigen-value problem". Therefore, to obtain the poles u_k we construct the following matrix equation:

$$\underline{U_K}^{-1}.\overline{U_K} = Q^{-1}.\Phi.Q. \tag{2.31}$$

Now by taking the Eigen-Value-Decomposition (EVD), we obtain the matrix Φ which is a diagonal matrix containing all the poles u_k:

$$eig(\underline{U_K}^{-1}.\overline{U_K}) = eig(Q^{-1}.\Phi.Q) = \Phi. \tag{2.32}$$

Moreover, since we have found the exact values of the poles u_k, we can now construct the matrices S and T to obtain the amplitudes a_k, using the following equation:

$$A = (S^{\dagger}).H.(T^{T})^{\dagger}, \tag{2.33}$$

where the dagger ($\dagger$) sign stands for pseudo-inverse of the matrix. It is important to mention that in the case of having multiple poles, for example $u_{k-1} = u_k$, the matrices S and T are rank deficient and the harmonic retrieval method is unable to find the poles u_k.

2.3 Multidimensional Sampling Framework

The problem of sampling two dimensional signals is more involved and does not allow direct extension of the 1-D results. Figure 2.2 shows the sampling setup used for sampling 2-D FRI signals. In the figure, $g(x, y)$ represents the input FRI signal, $\phi(x, y)$ the sampling kernel, $g_s(x, y)$ the sampled version of the input signal $g(x, y)$, $s_{j,k}$ the samples and T_x, T_y are the sampling intervals along the horizontal and vertical directions respectively. For

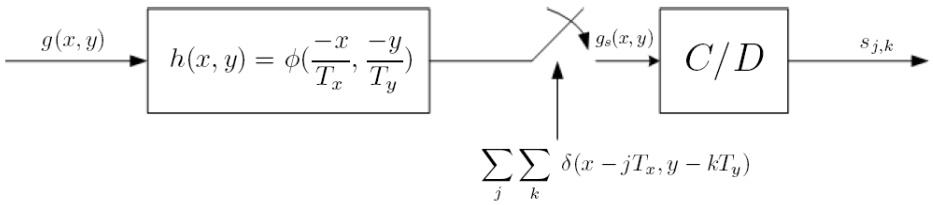

Figure 2.2: **2-D FRI sampling setup**

the sampling setup shown in Figure 2.2, the samples $s_{j,k}$ are given by:

$$s_{j,k} = \int_{-\infty}^{\infty} \int_{-\infty}^{\infty} g(x,y)\ \phi(\frac{x}{T_x} - j, \frac{y}{T_y} - k)\ dx\ dy \tag{2.34}$$

$$= \langle g(x,y), \phi(\frac{x}{T_x} - j, \frac{y}{T_y} - k)\rangle. \tag{2.35}$$

The definition of 2-D FRI signals is very similar to the 1-D case, that is 2-D signals with FRI have the following form:

$$g(x,y) = \sum_{r=0}^{N} \sum_{j\in\mathbb{Z}} \sum_{k\in\mathbb{Z}} \gamma_{j,k,r}\ \phi_r(x - x_j, y - y_k). \tag{2.36}$$

The degrees of freedom of the signal $g(x,y)$ are the shifts x_j, y_k and the coefficients $\gamma_{j,k,r}$, assuming that the set of functions $\phi_r(x,y)$ are known. If we introduce a counter which counts the number of free parameters of the signal $g(x,y)$ over the window of size (τ_x, τ_y), then the rate of innovation of the signal $g(x,y)$ is:

$$\rho = \lim_{\tau_x,\tau_y\to\infty} \frac{1}{\tau_x\tau_y} C_g \left[(-\tfrac{\tau_x}{2}, \tfrac{\tau_x}{2}), (-\tfrac{\tau_y}{2}, \tfrac{\tau_y}{2})\right]. \tag{2.37}$$

A set of 2-D Diracs, bilevel polygons and classes of algebraic curves (ellipses, cardioids and lemniscates) are all examples of 2-D signals with finite rate of innovation. Also, as in the 1-D case, all two dimensional bandlimited signals could be defined with the above definition.

The sampling kernels that we consider are given by the tensor product of two 1-D functions, that is: $\phi(x,y) = \phi(x) \otimes \phi(y)$. If two functions $\phi(x)$ and $\phi(y)$ can reproduce the polynomials x^m and y^n, then the resulting 2-D kernel can reproduce polynomials along x and y, that is:

$$\sum_{j\in\mathbb{Z}} \sum_{k\in\mathbb{Z}} c_{j,k}^{m,n} \phi(x - x_j, y - y_k) = x^m y^n, \tag{2.38}$$

for a proper choice of coefficients $c_{j,k}^{m,n}$ with $m = 0, 1, \ldots, M$ and $n = 0, 1, \ldots, N$. 2-D orthogonal Daubechies scaling functions [32] and 2-D biorthogonal B-splines [29], both satisfy the above property. Likewise, if $\phi(x)$ and $\phi(y)$ can reproduce exponentials, then:

$$\sum_{j\in\mathbb{Z}} \sum_{k\in\mathbb{Z}} c_{j,k}^{m,n} \phi(x - x_j, y - y_k) = e^{\alpha_m x} e^{\beta_n y}, \tag{2.39}$$

for a proper choice of coefficients $c_{j,k}^{m,n}$. E-splines [3] are included in the class of kernels that satisfy the property defined in equation (2.39).

In theory, like the 1-D case, the exponential or the polynomial moments can be used to retrieve the degrees of freedom of $g(x,y)$, however, the reconstruction of multidimensional FRI signals is more involved and requires tools such as complex moments [13], Radon transform [13, 10, 20] and 2-D harmonic retrieval methods [20]. In order to obtain the

moments from the samples, let us consider $\tau_{m,n}$ to be:

$$\tau_{m,n} = \sum_j \sum_k c_{j,k}^{m,n} \; s_{j,k}, \tag{2.40}$$

where $c_{j,k}^{m,n}$ are the suitable coefficients used in equations (2.38) or (2.39). By expanding $s_{j,k}$ we have:

$$\tau_{m,n} = \sum_j \sum_k c_{j,k}^{m,n} \; \langle g(x,y), \phi(x-j, y-k) \rangle \tag{2.41}$$

$$= \langle g(x,y), \sum_j \sum_k c_{j,k}^{m,n} \; \phi(x-j, y-k) \rangle, \tag{2.42}$$

where $g(x,y)$ is a non-zero and integrable function defined in the closed region Ω. Assuming that a polynomial reproducing kernel is used as the sampling kernel $\phi(x,y)$, then by substituting equation (2.38) into the above equation, the 2-D geometric moments of the signal are obtained:

$$\tau_{m,n} = \langle g(x,y), x^m \; y^n \rangle \tag{2.43}$$

$$= \int_{-\infty}^{\infty} \int_{-\infty}^{\infty} g(x,y) \; x^m \; y^n \; dx \; dy. \tag{2.44}$$

Likewise, if an exponential reproducing kernel is used as the sampling kernel, then by substituting equation (2.39), the exponential moments of the signal are obtained:

$$\tau_{m,n} = \langle g(x,y), e^{\alpha_m x} e^{\beta_n y} \rangle \tag{2.45}$$

$$= \int_{-\infty}^{\infty} \int_{-\infty}^{\infty} g(x,y) \; e^{\alpha_m x} e^{\beta_n y} \; dx \; dy. \tag{2.46}$$

It is important to note that, in the case of purely imaginary E-splines, the discrete Fourier coefficients of the signal $g(x,y)$ are obtained from the exponential moments, that is:

$$\tau_{m,n} = G[\alpha_m, \beta_n], \tag{2.47}$$

where $G(u,v)$ represents the Fourier transform of the signal $g(x,y)$. We will use this important fact in the next chapter.

Chapter 3

Sampling Multidimensional FRI Signals Using E-Splines

3.1 Introduction

As we have mentioned, E-spline sampling kernels have not been considered yet for the sampling of multidimensional FRI signals. In this chapter we present our novel algorithms for sampling and perfectly reconstructing 2-D stream of Diracs and bilevel polygons using E-spline sampling kernels.

3.2 Sampling and Reconstructing 2-D Diracs Using E-splines

Let us assume that a set of 2-D Diracs is passed through the sampling setup shown in Figure 2.2 with E-spline being the sampling kernel. As we have illustrated before, the exponential moments from the samples of a signal are given by:

$$\tau_{m,n} = \int_{-\infty}^{\infty}\int_{-\infty}^{\infty} g(x,y)\, e^{\alpha_m x} e^{\beta_n y}\, dx\, dy. \tag{3.1}$$

Assuming that there are K Diracs in the signal, such a signal can be represented as:

$$g(x,y) = \sum_{k=1}^{K} a_k\, \delta(x - x_k, y - y_k), \tag{3.2}$$

where a_k are the amplitudes and (x_k, y_k) are the horizontal and vertical coordinates of the Diracs respectively. Since each Dirac has an amplitude and also a horizontal and vertical location, the rate of innovation of the signal equals to $3K$. Now by substituting the equation for 2-D Diracs as the input signal $g(x,y)$, we obtain:

$$\tau_{m,n} = \sum_{k=1}^{K} a_k \int_{-\infty}^{\infty}\int_{-\infty}^{\infty} \delta(x - x_k, y - y_k)\, e^{\alpha_m x} e^{\beta_n y}\, dx\, dy\ , \tag{3.3}$$

which from the theory of integration of Dirac delta functions, leads to:

$$\tau_{m,n} = \sum_{k=1}^{K} a_k \, e^{\alpha_m x_k} e^{\beta_n y_k}. \tag{3.4}$$

The question here is whether we can extend the annihilating filter method to the 2-D case and apply the post-filtering on the observed measurements $\tau_{m,n}$. Unfortunately, as Maravic points out in her paper [20], the relation $\tau_{m,n} * h_{m,n} = 0$, where $h_{m,n}$ is the annihilating filter, has an infinite number of zeros over the complex field, therefore a simple extension to the 2-D case is not possible.

One way to tackle this problem is by setting the indices m and n to zero one at time and applying the annihilating filter method on both sets to find the values of x_k and y_k coordinates separately. That is:

$$\tau_{0,n} = \sum_{k=1}^{K} a_k \, e^{\beta_n y_k} \tag{3.5}$$

$$\tau_{m,0} = \sum_{k=1}^{K} a_k \, e^{\alpha_m x_k}. \tag{3.6}$$

Unfortunately, the estimated locations have to be paired and this is a combinatorial problem which may not have a unique solution. Namely, two different pairings may lead to the same samples $s_{j,k}$. Moreover, in the case of common coordinates between x_k and y_k, the annihilating filter method is unable to find the multiple poles, because of having non-unique filter coefficients (explained in the previous chapter).

In the case of harmonic retrieval method, a similar approach was recognized by Rao and Kung [15]. Again, like the above case, their method is only valid for 2-D signals that have no common frequencies between the x_k and y_k coordinates and also no matching technique is described for finding the correct pairings between the estimated coordinates. MEMP (Matrix Enhancement and Matrix Pencil) by Hua [14], addresses the two issues mentioned above, where in the case of having common coordinates, Hua solves the rank deficiency problem by enhancing the original data matrix. In this way, a partitioned and stacked Hankel matrix of the original data matrix is constructed in a way such that the full-rank property of the original matrix is restored. For the pairing problem, a combinatorial approach is suggested, trying all the possible combinations to find the correct pairing which is highly computational and not efficient.

The ACMP (Algebraically Coupled Matrix Pencils) method by F. Vanpoucke et al [7] uses a clever way to pair the frequencies by simultaneously solving two algebraically related generalized eigenvalue equations. As the matrix enhancement approach in [14] is not compatible with the algebraic pairing technique, they introduce an alternative rank restoration technique. In the next section we will describe the ACMP method and show how by the use of that method we are able to find the x_k and y_k coordinates and also the

amplitudes a_k from the exponential moments obtained from the samples. This method would also work for polynomial moments. Furthermore, in the Appendix, we present an extension to the ACMP method for various data models other than the standard data model used for harmonic retrieval methods [40, 18].

3.2.1 ACMP Method

Let us consider that we have access to the measurements $\tau_{m,n}$ which consists of a sum of K exponentials (complex or real) with unknown coordinate pairs x_k and y_k, and amplitudes a_k. The observed measurements $\tau_{m,n}$ obtained from sampling K 2-D Diracs with E-spline sampling kernels, can be rewritten as:

$$\tau_{m,n} = \sum_{k=1}^{K} a_k \; e^{\alpha_m x_k} \; e^{\beta_n y_k} \tag{3.7}$$

$$= \sum_{k=1}^{K} a_k . e^{\alpha_0 x_k} . e^{\beta_0 y_k} \; e^{\lambda_1 m x_k} e^{\lambda_2 n y_k} \tag{3.8}$$

$$= \sum_{k=1}^{K} \widehat{a_k} \varphi_k^m \; \psi_k^n, \tag{3.9}$$

where $\widehat{a_k} = a_k . e^{\alpha_0 x_k} . e^{\beta_0 y_k}$, $\varphi_k = e^{\lambda_1 x_k}$ and $\psi_k = e^{\lambda_2 y_k}$. In matrix form, the observed measurements $\tau_{m,n}$ can be written as a product of three matrices X_M, A and Y_N, that is

$$H_{M \times N} = X_M . A . Y_N^T, \tag{3.10}$$

where

$$H_{M \times N} = \begin{bmatrix} 1 & 1 & \dots & 1 \\ \varphi_1 & \varphi_2 & \dots & \varphi_K \\ \vdots & \vdots & \ddots & \vdots \\ \varphi_1^{M-1} & \varphi_2^{M-1} & \dots & \varphi_K^{M-1} \end{bmatrix} \begin{bmatrix} \widehat{a_1} & 0 & \dots & 0 \\ 0 & \widehat{a_2} & \dots & 0 \\ \vdots & \vdots & \ddots & \vdots \\ 0 & 0 & \dots & \widehat{a_K} \end{bmatrix} \begin{bmatrix} 1 & 1 & \dots & 1 \\ \psi_1 & \psi_2 & \dots & \psi_K \\ \vdots & \vdots & \ddots & \vdots \\ \psi_1^{N-1} & \psi_2^{N-1} & \dots & \psi_K^{N-1} \end{bmatrix}.$$

What we have here is very similar to the Hankel matrix defined in the 1-D case but unfortunately we can not simply extend the 1-D solution to the 2-D case because of the two following reasons:

1) Rank deficiency of matrix H when there are shared frequencies along the horizontal and vertical directions.

2) The pairing between the retrieved horizontal and vertical components is also an issue.

The ACMP approach by F. Vanpoucke et al [7] overcomes the two mentioned problems very efficiently. To describe the method, we start by solving the second problem first, so we will assume that there are no common coordinates along the pairs x_k and y_k. The matrices X_M and Y_N have a Vandermonde structure. From the shift-invariance property

of Vandermonde matrices, we have that $\overline{X_M} = \underline{X_M}.\Phi$ and $\overline{Y_N} = \underline{Y_N}.\Psi$ where the matrix Φ is a diagonal matrix containing all the x_k, Ψ is a diagonal matrix containing all the y_k, $\overline{X_M}$ and $\underline{X_M}$ denote the matrix X_M after the omission of the first and last row respectively (same for Y_N). From the Vandermonde structure of the matrices and their properties defined above, we obtain the following results for the four sub-matrices $H_{top-left}$, $H_{top-right}$, $H_{bottom-left}$ and $H_{bottom-right}$ of the Hankel matrix H. The four sub-matrices correspond to the omission of the first and last rows and columns of the data matrix H:

$$H_{tl} = \underline{H|} = \underline{X}.A.\underline{Y}^T \tag{3.11}$$

$$H_{tr} = \underline{|H} = \underline{X}.A.\overline{Y}^T = \underline{X}.(A.\Psi).\underline{Y}^T \tag{3.12}$$

$$H_{bl} = \overline{H|} = \overline{X}.A.\underline{Y}^T = \underline{X}.(\Phi.A).\underline{Y}^T \tag{3.13}$$

$$H_{br} = \overline{|H} = \overline{X}.A.\overline{Y}^T = \underline{X}.(\Phi.A.\Psi).\underline{Y}^T. \tag{3.14}$$

We can now construct two matrix pencil equations as follows:

$$H_{tr} - \mu.H_{tl} = \underline{X}.A.(\Psi - \mu.I)\underline{Y}^T \tag{3.15}$$

$$H_{bl} - \lambda.H_{tl} = \underline{X}.A.(\Phi - \lambda.I)\underline{Y}^T, \tag{3.16}$$

where the pairs (λ,μ) are called the rank reducing numbers and are equal to the poles (φ_k,ψ_k) we want to estimate. If there are no common coordinates along the horizontal or vertical directions, then each matrix pencil above would have a rank equal to K. Only if $\lambda = \varphi_K$ and $\mu = \psi_K$ the rank of the matrix would drop to $K-1$. We can use the method described for the one dimensional case to solve for φ_K and ψ_K separately but we would have a problem with the pairing of the estimated values. F.Vanpoucke et al [7] came up with the following algorithm to sort out the problem with the pairing of the estimated values: First the SVD of H_{tl} is computed as follows:

$$H_{tl} = U.\Sigma.V^H. \tag{3.17}$$

By multiplying U^H to the left hand side of the first matrix pencil defined in equation (3.15), and also multiplying V to the right hand side of the same matrix pencil, we obtain:

$$U^H.(H_{tr} - \mu.H_{tl}).V = U^H.H_{tr}.V - \mu.U^H.H_{tl}.V \tag{3.18}$$

$$= U^H.\underline{X}.A.\Psi.\underline{Y}^T.V - \mu.U^H.\underline{X}.A.\underline{Y}^T.V \tag{3.19}$$

$$= F.\Psi.G - \mu.F.G \tag{3.20}$$

$$= C_{tr} - \mu.C_{tl}, \tag{3.21}$$

where $F = U^H.\underline{X}.A$, $G = \underline{Y}^T.V$, $C_{tr} = F.\Psi.G$ and $C_{tl} = F.G$. Also with the same

multiplication on the second matrix pencil (equation (3.16)) we obtain:

$$U^H.(H_{bl} - \lambda.H_{tl}).V = U^H.H_{bl}.V - \lambda.U^H.H_{tl}.V \tag{3.22}$$
$$= U^H.\underline{X}.A.\Phi.\underline{Y}^T.V - \lambda.U^H.\underline{X}.A.\underline{Y}^T.V \tag{3.23}$$
$$= F.\Phi.G - \lambda.F.G \tag{3.24}$$
$$= C_{bl} - \lambda.C_{tl}. \tag{3.25}$$

Now we have constructed two new matrix pencils: $C_{tr} - \mu.C_{tl}$ and $C_{bl} - \lambda.C_{tl}$. By applying Eigen-Value-Decomposition on both matrix pencils, the poles φ_k and ψ_k are obtained:

$$eig(C_{tl}^{-1}.C_{tr}) = eig(G^{-1}.F^{-1}.F.\psi.G) = eig(G^{-1}.\psi.G) = \Psi. \tag{3.26}$$
$$eig(C_{tl}^{-1}.C_{bl}) = eig(G^{-1}.F^{-1}.F.\varphi.G) = eig(G^{-1}.\varphi.G) = \Phi. \tag{3.27}$$

The identical transformation G on both equations will guarantee us to have the correct pairing for the estimated φ_k and ψ_k values. This algorithm is also very efficient as we need to calculate the transformation parameter G once from the first matrix pencil, and apply that to the second matrix pencil. Moreover, as $U^H.H_{tl}.V = F.G = C_{tl} = \Sigma$, inverting C_{tl}, which is just a diagonal matrix, is not computationally expensive.

The algorithm we just explained will fail if there are multiple frequency pairs with one coordinate in common because of the rank deficiency of X_M and/or Y_N matrices. As we mentioned before, Hua [14] constructs an enhanced matrix by partitioning and stacking the original data matrix such that the enhanced matrix is of rank K. A similar approach is used in the ACMP method but with a different restoration technique so that the enhanced matrix will be compatible with the pairing technique. The rank-restoration technique is as follows:

Consider the matrix $H^{l,k}$ to be:

$$H^{(l,k)} = H_{l:K+l,k:K+k}. \tag{3.28}$$

Also let us define the enhanced matrix J of size $K(K+1) \times K(K+1)$ to be:

$$J = \begin{bmatrix} H^{(1,1)} & H^{(2,1)} & \dots & H^{(K,1)} \\ H^{(1,2)} & H^{(2,2)} & \dots & H^{(K,2)} \\ \vdots & \vdots & \ddots & \vdots \\ H^{(1,D)} & H^{(2,D)} & \dots & H^{(K,K)} \end{bmatrix}.$$

For the construction of matrix J, we need at least $2K \times 2K$ data points. The described matrix J has very similar properties to the Hankel matrix H and can be decomposed as follows:

$$J = X'.A.Y'^T, \tag{3.29}$$

where

$$X' = \begin{bmatrix} X_{K+1}^T & \Psi.X_{K+1}^T & \Psi^2.X_{K+1}^T & \dots & \Psi^{K-1}.X_{K+1}^T \end{bmatrix}^T \tag{3.30}$$

$$Y' = \begin{bmatrix} Y_{K+1}^T & \Phi.Y_{K+1}^T & \Phi^2.Y_{K+1}^T & \dots & \Phi^{K-1}.Y_{K+1}^T \end{bmatrix}^T, \tag{3.31}$$

and

$$X_{K+1} = \begin{bmatrix} 1 & 1 & \dots & 1 \\ \varphi_1 & \varphi_2 & \dots & \varphi_K \\ \vdots & \vdots & \ddots & \vdots \\ \varphi_1^K & \varphi_2^K & \dots & \varphi_K^K \end{bmatrix} \quad Y_{K+1} = \begin{bmatrix} 1 & 1 & \dots & 1 \\ \psi_1 & \psi_2 & \dots & \psi_K \\ \vdots & \vdots & \ddots & \vdots \\ \psi_1^K & \psi_2^K & \dots & \psi_K^K \end{bmatrix}.$$

The matrices X' and Y' have a Vandermonde structure and for the coinciding φ_k, the corresponding ψ_k will be different and therefore both matrices are full rank if the matrix J is at least of size $K(K+1) \times K(K+1)$. Recalling the shift-invariant property for Vandermonde matrices, we have: $\overline{\overline{X'}} = \underline{\underline{X'}}.\Phi$ and $\overline{\overline{Y'}} = \underline{\underline{Y'}}.\Psi$ where

$$\underline{\underline{X'}} = \begin{bmatrix} \underline{X_{K+1}^T} & \Psi.\underline{X_{K+1}^T} & \Psi^2.\underline{X_{K+1}^T} & \dots & \Psi^{K-1}.\underline{X_{K+1}^T} \end{bmatrix}^T. \tag{3.32}$$

$$\overline{\overline{X'}} = \begin{bmatrix} \overline{X_{K+1}^T} & \Psi.\overline{X_{K+1}^T} & \Psi^2.\overline{X_{K+1}^T} & \dots & \Psi^{K-1}.\overline{X_{K+1}^T} \end{bmatrix}^T. \tag{3.33}$$

As we have mentioned before, $\overline{X}$ and $\underline{X}$ denote the matrix X after omission of the first and last row respectively (same for the matrix Y'). Now we can apply the previous algorithm on the matrix J, however, the process of omitting rows and columns has to be applied to the block components of matrix J. Again, due to the Vandermonde structure of matrices Y' and X', the four sub-matrices $J_{top-left}$, $J_{top-right}$, $J_{bottom-left}$ and $J_{bottom-right}$ of matrix J are constructed, which correspond to the omission of the first and last rows and columns on each block of the matrix J:

$$J_{tl} = \underline{\underline{X'}}.A.\underline{\underline{Y'}}^T \tag{3.34}$$

$$J_{tr} = \underline{\underline{X'}}.A.\overline{\overline{Y'}}^T = \underline{\underline{X'}}.A.\Psi.\underline{\underline{Y'}}^T \tag{3.35}$$

$$J_{bl} = \overline{\overline{X'}}.A.\underline{\underline{Y'}}^T = \underline{\underline{X'}}.\Phi.A.\underline{\underline{Y'}}^T \tag{3.36}$$

$$J_{br} = \overline{\overline{X'}}.A.\overline{\overline{Y'}}^T = \underline{\underline{X'}}.\Phi.A.\Psi.\underline{\underline{Y'}}^T. \tag{3.37}$$

From the matrices described above we can obtain two matrix pencils, that is: $J_{tr} - \mu.J_{tl}$ and $J_{bl} - \lambda.J_{tl}$. Now with the use of EVD, we can calculate for φ_k and ψ_k as explained previously. Moreover, since we have found the exact values of the poles φ_k and ψ_k, we can now construct the matrices X' and Y' to obtain the parameters $\widehat{a_k}$, using the following equation:

$$A = (X'^{\dagger}).H.(Y'^T)^{\dagger}. \tag{3.38}$$

From the estimated parameters $\widehat{a_k}$ and the poles φ_k and ψ_k we can easily find the ampli-

tudes a_k:

$$a_k = \frac{e^{\alpha_0 x_k}.e^{\beta_0 y_k}}{\widehat{a_k}}. \tag{3.39}$$

3.2.2 A Sampling Theorem For Reconstructing 2-D Diracs Using E-Splines

In the previous section it was shown that by using the ACMP method we can recover the coordinates x_k, y_k and the amplitudes a_k from exponential moments of 2-D stream of Diracs obtained from the samples. It was also shown that, for a stream of K 2-D Diracs, at least $2K \times 2K$ data points are required for the construction of the enhanced matrix. Therefore we need the 2-D exponential spline order to be at least $2K-1 \times 2K-1$ in order to produce the $2K \times 2K$ exponential moments. Figure 3.1 shows an example, where the input signal, its corresponding 16×16 samples and the reconstructed signal are all shown. We can now summarize the above discussion with the following proposition:

Proposition I - A set of K 2-D Diracs is uniquely determined from the samples $s_{j,k} = \langle g(x,y), \phi(\frac{x}{T_x} - j, \frac{y}{T_y} - k)\rangle$ provided that the sampling kernel $\varphi(x,y)$ can reproduce exponentials with an order $2K-1 \times 2K-1$.

3.3 Sampling and Reconstructing Bilevel Polygons Using E-splines

Consider a non-intersecting, convex and bilevel N-sided polygon with vertices at points (x_i, y_i), $i = 1, 2, \ldots, N$, which is sampled with E-spline sampling kernel. The described polygon can be uniquely specified by its N vertices and therefore it has a rate of innovation equal to $2N$. Sampling and perfectly reconstructing bilevel polygons with E-splines has not been considered yet and in this section we will present a novel algorithm for reconstructing bilevel polygons with the use of E-splines. The Fourier transform of bilevel polygons, Radon transform and projection-slice theorem [17] are all utilized to perfectly reconstruct sampled bilevel polygons. At first we will show how the Fourier transform of bilevel polygons is represented.

3.3.1 Fourier Transform of a Polygonal Shape Function

As we have mentioned before, sampling signals with E-splines would result in having the exponential moments of the input signal, using the equation $\tau_{m,n} = \sum_j \sum_k c_{j,k}^{m,n} s_{j,k}$.

S.Lee and R.Mittra [6] derived an expression for the Fourier transform of any N-sided bilevel polygon. To briefly describe their solution, let us assume that Σ is an N-sided bilevel polygon as shown in Figure 3.2. In the figure, the numbers $i = 1, 2, \ldots, N$ represent the vertices of the polygon, O represents a relative origin and p_i represent the gradient of

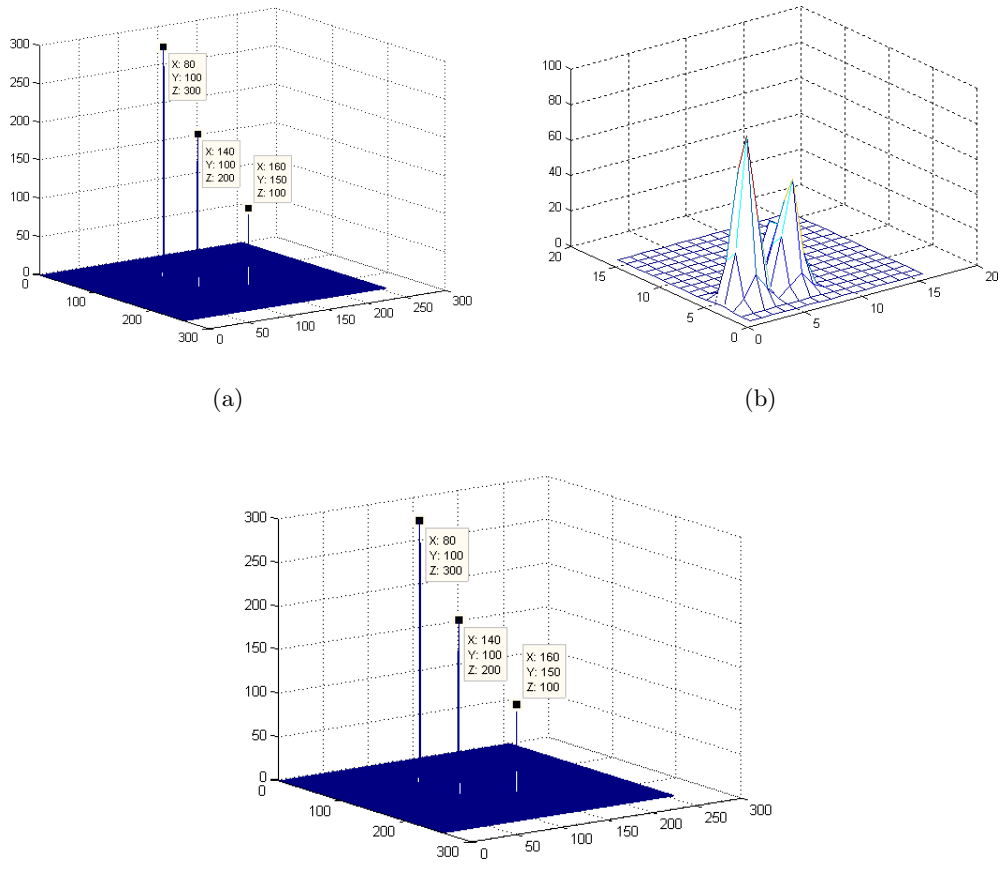

(a) (b)

(c)

Figure 3.1: **Sampling and reconstructing 2-D Diracs using E-splines (a) The original input signal consisting of 3 Diracs in a frame size of 256×256 with locations $(\mathbf{x_k}, \mathbf{y_k}) = [(\mathbf{150}, \mathbf{160}), (\mathbf{100}, \mathbf{140}), (\mathbf{100}, \mathbf{80})]$ and amplitudes $(\mathbf{100}, \mathbf{200}, \mathbf{300})$ respectively. (b) The $\mathbf{16 \times 16}$ samples of the original signal (c) The reconstructed signal with the use of ACMP algorithm with the retrieved locations $(\mathbf{x_k}, \mathbf{y_k}) = [(\mathbf{150}, \mathbf{160}), (\mathbf{100}, \mathbf{140}), (\mathbf{100}, \mathbf{80})]$ and amplitudes $(\mathbf{100}, \mathbf{200}, \mathbf{300})$ respectively.**

the polygon's sides. Let us also define the polygon function $g(x, y)$ of Σ as:

$$g(x,y) = \begin{cases} 1 & \text{if } (x,y) \text{ is in } \Sigma \\ 0 & \text{otherwise.} \end{cases} \tag{3.40}$$

From literature we know that the Fourier transform of any 2-D function $g(x, y)$ is defined as:

$$G(u,v) = \int_{-\infty}^{\infty} \int_{-\infty}^{\infty} g(x,y)\, e^{jux}\, e^{jvy}\, dx\, dy. \tag{3.41}$$

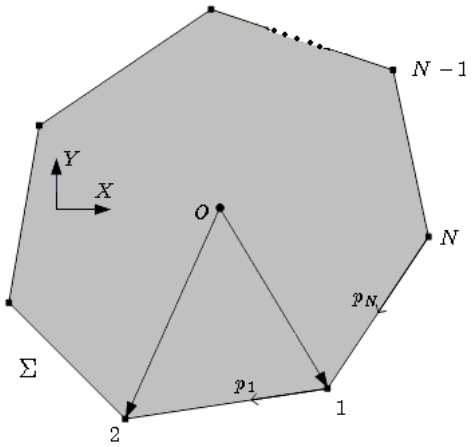

Figure 3.2: **N-sided polygon**

S.Lee and R.Mittra showed that the Fourier transform of any N-sided bilevel polygon is:

$$G(u,v) = \sum_{i=1}^{N} e^{j(ux_i+vy_i)} \frac{p_{i-1} - p_i}{(u + p_{i-1}v).(u + p_iv)}, \tag{3.42}$$

where (x_i, y_i) are the locations of the vertices of the polygon. This result shows that the Fourier transform of bilevel polygons is directly dependent on the location of the vertices of the polygons. The reader can refer to [6] for the derivation of this result.

As can be seen from the above equation, the Fourier transform of an N-sided bilevel polygon, closely follows the data model used for 2-D harmonic retrieval [7] methods (ACMP method for example). However, since the result for the Fourier transform has a frequency-varying amplitude, we cannot simply apply 2-D harmonic retrieval methods to find the locations (x_i, y_i). Having said that, by setting u and v to zero separately, we will end up with two equations in power-series form. Therefore we can find the values of x_i and the values of y_i separately. Unfortunately, in this way, there will be a problem with the pairing of x_i and y_i values. Fortunately, with the use of the connection between the Fourier transform and Radon transform, also know as the projection-slice theorem [17], we can efficiently retrieve the locations of the vertices of bilevel polygons. Next, we will give a brief introduction of the Radon transform and its connection with the Fourier transform.

3.3.2 Introduction to Radon Transform

The Radon transform is used in diverse fields of applications such as computed tomography, astronomy, optics, geophysics and many other areas [8]. In this section we take advantage of the connection between the Radon transform and Fourier transform, to sample and perfectly reconstruct bilevel polygons.

The Radon transform $R_g(t, \theta)$ of a two dimensional, continuous, square integrable function $g(x, y)$ defined in a closed region Ω, is found by integrating g along lines with angle θ over the x-axis. The projections $R_g(t, \theta)$ or the line integrals along each $\theta \in [0, \pi)$ will

result in 1-D functions with finite support. The collection of $R_g(t,\theta)$ at all θs is called the Radon transform of $g(x,y)$, that is:

$$R_g(t,\theta) = \int_{-\infty}^{\infty} \int_{-\infty}^{\infty} g(x,y)\ \delta(t - x\cos(\theta) - y\sin(\theta))\ dx\ dy \tag{3.43}$$

There are many methods to reconstruct the original function $g(x,y)$ from the projections

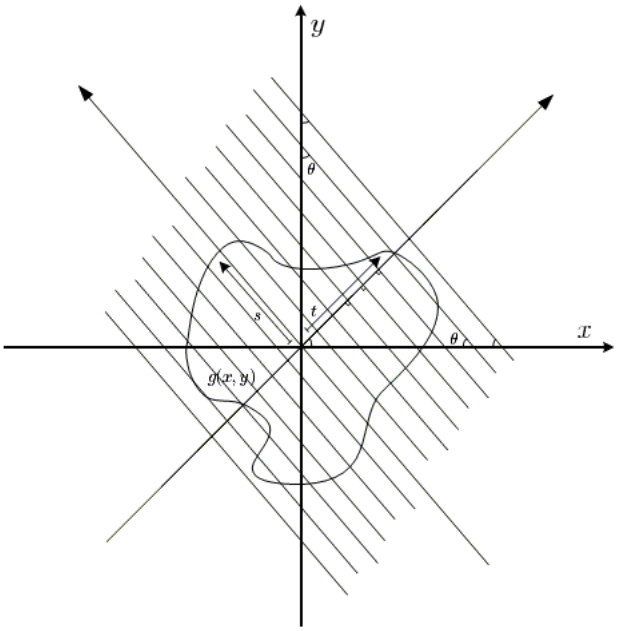

Figure 3.3: **Line integrals at an angle θ**

[8] but the most popular is the filtered-backprojection algorithm [8].

3.3.3 Projection-Slice Theorem

The input function $g(x,y)$ must be a square integrable function with finite support. An important result [9] which is derived from the definition of the Radon transform is that if $F(t)$ is a square-integrable function then the following relation holds true:

$$\int_{-T}^{T} R_g(t,\theta)\ F(t)\ dt = \int\int_{\Omega} F(x\cos(\theta) + y\sin(\theta))\ dx\ dy, \tag{3.44}$$

where T is the maximal support value of the closed region Ω in the direction θ. By considering $F(t) = e^{-j\omega t}$, a direct relationship between the 2-D Fourier transform and the Radon transform is observed. The derivation is as follows: If $F(t) = e^{-j\omega t}$ then:

$$F(xcos(\theta) + ysin(\theta)) = e^{-j\omega(x\cos(\theta)+y\sin(\theta))}, \tag{3.45}$$

by taking the 1-D Fourier transform of the Radon transform $R_g(t,\theta)$, we obtain:

$$\hat{R}_g(\omega,\theta) = \int_{-\infty}^{\infty} R_g(t,\theta)\, e^{-j\omega t}\, dt \tag{3.46}$$

$$= \int\int_{\Omega}\int_{-\infty}^{\infty} g(x,y)\, e^{-j\omega t}\, \delta(t - x\cos(\theta) - y\sin(\theta))\, dx\, dy\, dt \tag{3.47}$$

$$= \int\int_{\Omega} g(x,y)\, e^{-j\omega x\cos(\theta)}\, e^{-j\omega y\sin(\theta)}\, dx\, dy. \tag{3.48}$$

Going back to the definition of the Fourier transform of a 2-D function $g(x,y)$ and by comparing it with the 1-D Fourier transform of the Radon transform of $g(x,y)$, we observe that:

$$G(\omega\cos(\theta), \omega\sin(\theta)) = \hat{R}_g(\omega,\theta). \tag{3.49}$$

What we have shown here is also known as the projection-slice theorem. We can see that the Fourier transform function $G(u,v)$ evaluated along a line passing through the origin at an angle θ in Fourier domain, is identical to the one dimensional Fourier transform of the projection $R_g(t,\theta)$, where the projection angle is at the same angle θ. Therefore the Radon transform is closely related to the Fourier transform. In the next section, we will show how with the use of the projection-slice theorem we can perfectly retrieve the locations of the vertices of bilevel polygons.

3.3.4 A Sampling Theorem For Reconstructing Bilevel Polygons Using E-Splines

In this section we will present a novel algorithm for reconstructing bilevel polygons with the use of E-splines. To start, let us assume that a bilevel N-sided polygon has been sampled with E-spline sampling kernel. So the sample $s_{m,n}$ are given by:

$$s_{m,n} = \langle g(x,y), \phi(x-m, y-n\rangle.$$

Using equation (2.40) we obtain the exponential moments of the signal from the samples $s_{m,n}$:

$$\tau_{m,n} = \int_{-\infty}^{\infty}\int_{-\infty}^{\infty} g(x,y)\, e^{\alpha_m x} e^{\beta_n y}\, dx\, dy.$$

Furthermore, as we mentioned earlier on, the Fourier transform of any polygon can be written as [6]:

$$G(u,v) = \sum_{i=1}^{N} e^{j(ux_i + vy_i)}\, \frac{p_{i-1} - p_i}{(u + p_{i-1}v).(u + p_i v)}.$$

Therefore, from the equations shown above we can deduce the following:

$$\tau_{m,n} = G[m,n] \tag{3.50}$$

$$= \sum_{i=1}^{N} e^{(\alpha_m x_i + \beta_n y_i)} \ \frac{p_{i-1} - p_i}{(m + p_{i-1}n).(m + p_i n)}, \tag{3.51}$$

that is, from the exponential moments of the signal we have access to the Fourier coefficients of the signal. Also, from the projection-slice theorem we know that the Fourier transform of a 2-D function $g(x, y)$ and the 1-D Fourier transform of the Radon transform of the same 2-D function are directly related, which in terms of discrete coefficients we have the following relationship:

$$G[\omega\cos(\theta), \omega\sin(\theta)] = \hat{R}_g[\omega, \theta], \tag{3.52}$$

where $\omega = \sqrt{m^2 + n^2}$ and $\theta = tan^{-1}(\frac{n}{m})$. By using this mapping, we can transform the Discrete Fourier transform of bilevel polygons obtained from the samples to the Radon domain as follows:

$$\tau_{\omega.cos(\theta),\, \omega.sin(\theta)} = \sum_{i=1}^{N} e^{x_i.\alpha_{\omega cos(\theta)} + y_i.\beta_{\omega sin(\theta)}} \ \frac{p_{i-1} - p_i}{\omega^2(cos(\theta) + p_{i-1}sin(\theta)).(cos(\theta) + p_i sin(\theta))}, \tag{3.53}$$

which, by assuming that $a_{i,\theta}$ is $\frac{p_{i-1}-p_i}{(cos(\theta)+p_{i-1}sin(\theta)).(cos(\theta)+p_i sin(\theta))}$, the equation above can be simplified to:

$$\tau_{\omega.cos(\theta),\, \omega.sin(\theta)} \times \omega^2 = \sum_{i=1}^{N} a_{i,\theta} \times e^{x_i.\alpha_{\omega cos(\theta)} + y_i.\beta_{\omega sin(\theta)}}. \tag{3.54}$$

Let us introduce $\widehat{\tau}_{\omega,\theta} = \tau_{\omega.cos(\theta),\omega.sin(\theta)} \times \omega^2$ to present the new mapped equation. At $\omega = 0$, $\widehat{\tau}_{\omega,\theta} = 0$, therefore the minimum required spline order can be decreased by 1 as the first data sample is always zero. The above equation can be rewritten as:

$$\widehat{\tau}_{\omega,\theta} = \sum_{i=1}^{N} a_{i,\theta} \times e^{x_i.\alpha_{\omega cos(\theta)} + y_i.\beta_{\omega sin(\theta)}}, \qquad \omega \neq 0. \tag{3.55}$$

Since θ is fixed for a given projection, i.e. $a_{i,\theta} = a_i$, the mapped equation at different Radon projections has the following form:

$$\widehat{\tau}_{\omega,\theta} = \sum_{i=1}^{N} \widehat{a_i}.e^{\omega z_i} = \sum_{i=1}^{N} \widehat{a_i}.(u_i)^{\omega}, \tag{3.56}$$

where $\widehat{a_i} = a_i.e^{\alpha_0 x_i}.e^{\beta_0 y_i}$, $z_i = x_i.cos(\theta).\lambda_1 + y_i.sin(\theta).\lambda_2$ and $u_i = e^{z_i}$. Some examples with

different θ are given below (derived from the fact that $\omega = \sqrt{m^2 + n^2}$ and $\theta = tan^{-1}(\frac{n}{m})$):

$$\begin{aligned} \widehat{\tau}_{\omega,0} &= \tau_{m,0} \times m^2 &&= \sum_{i=1}^{N} e^{x_i.\alpha_m} \ \frac{p_{i-1}-p_i}{1} \\ \widehat{\tau}_{n,\frac{\pi}{2}} &= \tau_{0,n} \times n^2 &&= \sum_{i=1}^{N} e^{y_i.\beta_n} \ \frac{p_{i-1}-p_i}{p_{i-1}.p_i} \\ \widehat{\tau}_{\omega,\frac{\pi}{4}} &= \tau_{m,m} \times 2m^2 &&= \sum_{i=1}^{N} e^{x_i.\alpha_m + y_i.\beta_m} \ \frac{p_{i-1}-p_i}{\frac{1}{2}.(1+p_{i-1}).(1+p_i)}. \end{aligned} \tag{3.57}$$

By using Prony's method, we can find all the parameters z_i for each projection. By back-projecting the parameters z_i according to their θ we are able to retrieve some information about the polygon's vertices. The question here is that how many projections will definitely guarantee us to perfectly reconstruct the polygon? This question was addressed by Maravic in [10] and she showed that $N + 1$ projections uniquely specify the locations of the vertices of the polygons. The same argument can be applied to Diracs as shown in Figure 3.4. Figure 3.4(a) shows an image with $N = 3$ Diracs and 3.4(b) shows $N + 1 = 4$ back-projections at angles 0, 90, 45 and $tan^{-1}(2)$ of the same image. It can be seen that exactly $N + 1 = 4$ lines intersect at the locations of the $N = 3$ Diracs. Thus, points that have $N + 1$ line intersections correspond to the N Diracs.

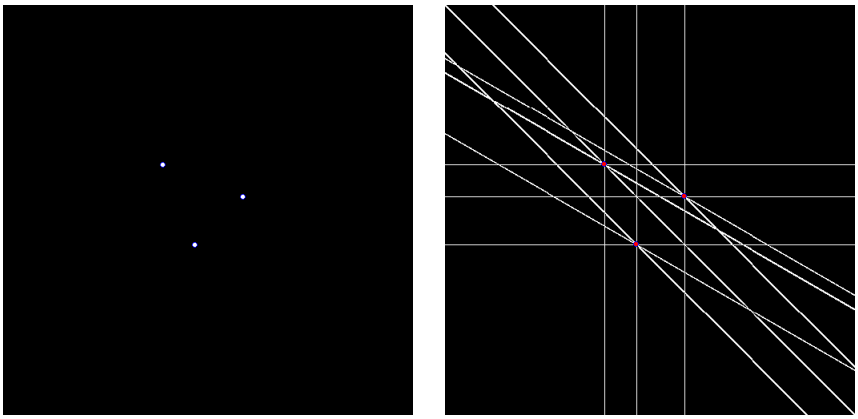

(a) (b)

Figure 3.4: **$\mathbf{K+1}$ projections for K 2-D Diracs completely specifies the signal (a) $\mathbf{g(x,y)}$ containing 3 Diracs (b) $\mathbf{3+1=4}$ back-projections**

Now let us consider that the input signal is a bilevel triangle. Using the sampling setup shown in Figure 2.2, the input signal is sampled at a rate $T = T_x = T_y$ with E-splines. Then, the exponential moments of the signal are calculated using equation (2.40). For the perfect reconstruction of the polygon, $3 + 1 = 4$ projections are required. As the first data sample is always zero, the number of measurements $\widehat{\tau}_{\omega,\theta}$ need to be at least $2N - 1 = 5$ for each projection angle θ. To retrieve the z_i parameters of each of the first 4 available projections, that is 0, 90, 45 and $tan^{-1}(2)$, we need the spline order to be at least $p(2N - 2) \times p(2N - 2)$. Here, p is the number required in order to produce at least $N+1$ projections. The value of p can be found by inspection but it can be shown that the

order of the spline required is $\mathcal{O}(N^2)$. For sampling and perfectly reconstructing bilevel triangles we need the spline order to be at least 8×8 and for 4-sided bilevel polygons we need the spline order to be at least 12×12 (by inspection).

Figure 3.5(a) shows a triangle in a frame size of 256×256. The signal is sampled at a rate $T_x = T_y = 8$ using real E-spline of order 8. The projections are taken at the angles 0, 90, 45 and $tan^{-1}(2)$. Using Prony's method, z_i parameters are recovered for each projection, normalized by $\sqrt{(m^2 + n^2)}$ and then back-projected according to their projection angle. Figure 3.5(b) shows the reconstructed signal where the crosses are the actual vertices of the original signal. We can see that our algorithm has perfectly reconstructed the locations of the vertices of the triangle.

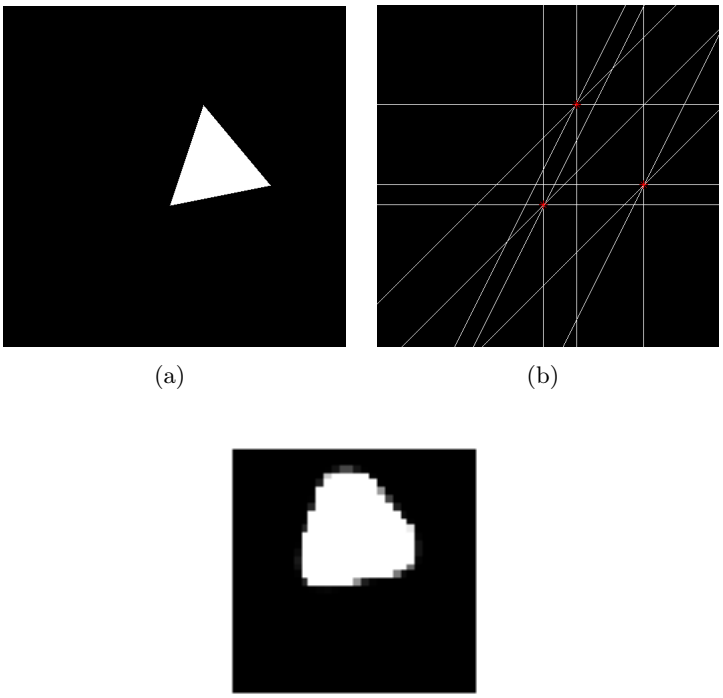

(a) (b)

(c)

Figure 3.5: **Sampling and Reconstructing a bilevel triangle using real E-splines (a) The original bilevel triangle (b) The reconstructed vertices where the crosses are the actual vertices of the original signal. (c) The 32×32 samples of the signal [Not to scale]**

To show another example, assume that we have a 4-sided bilevel polygon in a frame size of 512×512 (Figure 3.6(a)). The signal is sampled at a rate $T_x = T_y = 16$ using real E-spline of order 12. The projections are taken at the angles 0, 45, 90, $tan^{-1}(2)$ and $tan^{-1}(\frac{1}{2})$. Figure 3.6(b) shows the reconstructed signal where the crosses are the actual vertices of the original signal. As can be seen from the reconstructed image, not all the back-projected lines align at the vertices points. Instead of using real E-splines we can use purely imaginary E-splines which make the reconstruction more stable. Figure 3.7 shows the same image but now sampled with imaginary E-splines. To summarize our results, an

N-sided bilevel polygon is perfectly reconstructed from the samples $s_{j,k} = \langle g(x,y), \phi(\frac{x}{T_x} - j, \frac{y}{T_y} - k)\rangle$ provided that the sampling kernel $\varphi(x,y)$ can reproduce exponentials with an order $p(2N-2) \times p(2N-2)$, where p is the number required in order to produce at least $N+1$ projections.

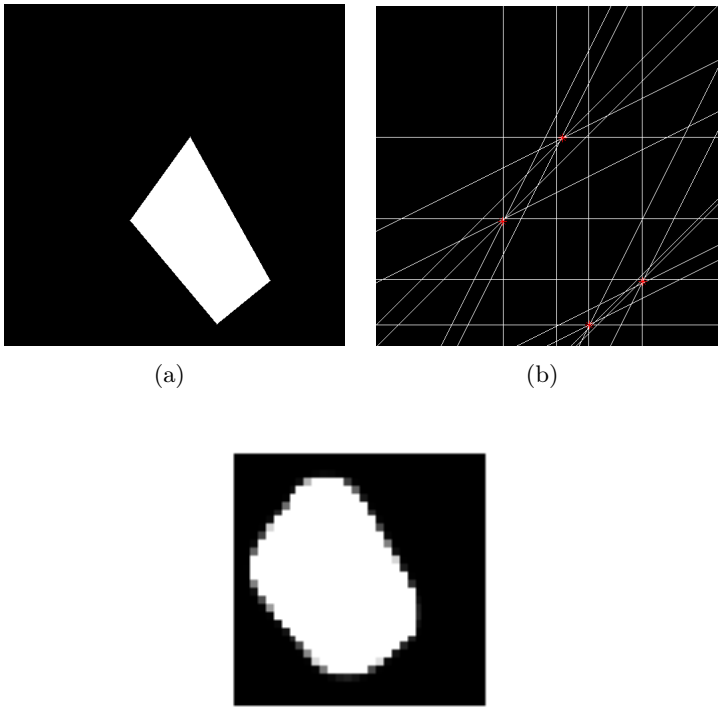

(a) (b)

(c)

Figure 3.6: **Sampling and Reconstructing a 4-sided bilevel polygon using real E-splines (a) The original 4-sided bilevel polygon (b) The reconstructed vertices where the crosses are the actual vertices of the original signal (c) The 32×32 samples of the signal [Not to scale]**

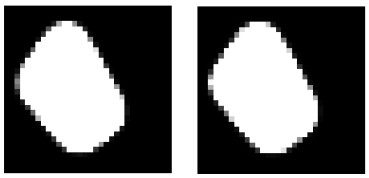

(a)

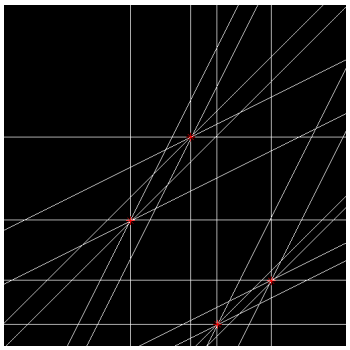

(b)

Figure 3.7: **Sampling and Reconstructing a 4-sided bilevel polygon using purely imaginary E-splines (a) The 32×32 real (left) and imaginary (right) samples of the signal shown in Figure 3.6 (b) The reconstructed vertices where the crosses are the actual vertices of the original signal. [Not to scale]**

Chapter 4

Multichannel Sampling of FRI Signals with E-Splines

4.1 Introduction

Imagine a multichannel sampling system consisting of many acquisition devices observing an input signal. In order to perfectly reconstruct the input signal using only one acquisition device, we normally require expensive acquisition devices with high sampling rates. By using a bank of acquisition devices (filters) and synchronizing the different channels exactly, we are able to reduce the number of samples needed from each device, resulting in a cheaper and more efficient sampling system. To model our multichannel system, consider a bank filters to acquire FRI signals where each filter has access to a delayed version of the input signal. Figure 4.1 shows a 1-D model for the described multichannel sampling scenario where the bank of filters $\varphi_1(x), \varphi_2(x), \ldots, \varphi_{N-1}(x)$ receive different delayed versions of the input signal $g_0(x)$. Here, the delays are denoted by $\mathcal{T}_1, \mathcal{T}_2, \ldots, \mathcal{T}_{N-1}$. Multichannel sampling aims to have filters of lower order and since less samples are needed from each sensor, the support of the corresponding sampling kernels are also reduced.

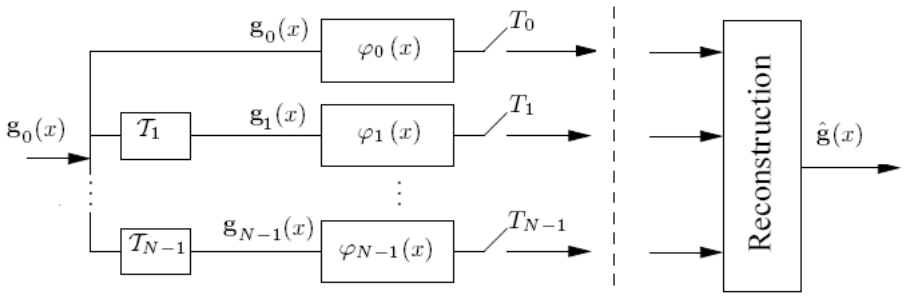

Figure 4.1: **1-D multichannel sampling scenario**

Multichannel sampling can be done in two ways, either symmetrically or non-symmetrically. A symmetric multichannel sampling system, which is of more interest in our research area, is a sampling setup in which the sampling is evenly distributed between different acquisi-

tion devices, while for the non-symmetric case, the reference signal is independently sent for perfect reconstruction and other acquisition devices only send the relevant samples that are needed to achieve perfect reconstruction. Multichannel sampling of bilevel polygons with polynomial reproducing kernels, in a non-symmetric manner, have been considered by Baboulaz [11]. He also looked at the case of multichannel sampling of a stream of 1-D Diracs using E-splines, which he shows that, unlike the polynomial reproducing kernels, we can truly distribute the acquisition of FRI signals. In this chapter we will show how by retrieving the delay parameters, we can symmetrically sample and reconstruct a given FRI signal. It will be shown that, by registering the delay parameters from the relevant features of the image samples, it is possible to synchronize the different channels exactly so that perfect reconstruction of the original input signal and its delayed versions is achieved.

4.2 Multichannel Sampling of 1-D Diracs

As mentioned before, we can truly distribute the acquisition of FRI signals with kernels reproducing exponentials. This is because, exponential splines can offer different kernels with the same order due to the arbitrary choice of the parameters α_0 and λ in $\alpha_m = \alpha_0 + m\lambda$. We will briefly explain Baboulaz's result [11] for 1-D Diracs and in the next sections we will show how we can extend his method to the two dimensional case.

Assume that we have two signals consisting of K Diracs, of which, one is a shifted version of the other, that is $x_1(t) = x_0(t - \Delta x)$ where Δx is the unknown shift between the two signals. The exponential moments for both sensors are given by:

$$\tau_m^0 = \int_{-\infty}^{\infty} x_0(t) e^{\alpha_m^0 t} dt \tag{4.1}$$

$$\tau_m^1 = \int_{-\infty}^{\infty} x_1(t) e^{\alpha_m^1 t} dt, \tag{4.2}$$

where superscripts 0 and 1 on the exponential moments τ_m^0 and τ_m^1 represent the reference sensor and the adjacent sensor respectively. Now assume that one parameter is common between the sets $\underline{\alpha^0}$ and $\underline{\alpha^1}$, for example the last parameter of the first sensor and the first parameter of the second sensor, that is: $\alpha_P^0 = \alpha_0^1 = \alpha$. The corresponding moments are:

$$\tau_P^0 = \int_{-\infty}^{\infty} x_0(t) e^{\alpha t} dt \tag{4.3}$$

$$\tau_0^1 = \int_{-\infty}^{\infty} x_1(t) e^{\alpha t} dt = \int_{-\infty}^{\infty} x_0(t - \Delta x) e^{\alpha t} dt, \tag{4.4}$$

which with simple rearrangements, leads to:

$$\tau_0^1 = e^{\alpha \Delta x} . \tau_P^0. \tag{4.5}$$

By taking logarithms on both sides we can easily find the shift parameter Δx as follows:

$$\ln\left(\frac{\tau_0^1}{\tau_P^0}\right) = \alpha.\Delta x. \tag{4.6}$$

From the estimated shift parameter Δx we can now easily find the higher moments of the first sensor from the second sensor and also the lower moments of the second sensor from the first sensor. To make things clearer, let us assume that we have $K = 2$ Diracs for our first signal and a shifted version of it for the second signal. From [2] we know that for a given K Diracs as the input signal, we need the E-spline order to be at least $2K - 1$, which means the sampling kernel needs to produce at least $2K$ exponentials. Assuming that $K = 2$, then the sampling kernel needs to produce at least 4 exponentials with $\underline{\alpha} = (\alpha_0, \alpha_1, \alpha_2, \alpha_3)$. Let us assume that $P = \alpha_2 = \alpha$ is the common parameter set between the two sensors. Moreover, with this arrangement, the $\underline{\alpha}^0$ set for the first sensor will be $\underline{\alpha}_0 = (\alpha_0, \alpha_1, \alpha_2)$ and for the second sensor: $\underline{\alpha}_1 = (\alpha_2, \alpha_3)$. As we have a common parameter between the two sets, the shift Δx can be calculated, as explained before. The exponential moments from the first sensor are now $(\tau_0^0, \tau_1^0, \tau_2^0)$ and its higher moments can be obtained from the moments of the second sensor, as follows: $(\tau_2^0, \tau_3^0) = (\tau_0^1.e^{-\alpha_2\Delta x}, \tau_1^1.e^{-\alpha_3\Delta x})$. Therefore we have all the $2K$ moments in order to reconstruct the signal from the first sensor. The same rule can be applied to the second sensor in order to obtain its lower moments from the moments of the first sensor. From [2] we know that a stream of Diracs is uniquely determined from the samples if there are at most K Diracs in an interval size of $2KLT$ where L is the support of the sampling kernel. Since the support of the sampling kernels is reduced in the multichannel case, then for a fixed T we can achieve a better performance for the multichannel case.

4.3 Multichannel Sampling of Multidimensional FRI Signals

A model of a 2-D multichannel system is shown in Figure 4.2 where the bank of E-spline filters $\varphi_1(x,y), \varphi_2(x,y), \ldots, \varphi_{N-1}(x,y)$ receive different delayed versions of the input 2-D signal $g_0(x,y)$ and the delays are denoted by $\mathcal{T}_1, \mathcal{T}_2, \ldots, \mathcal{T}_{N-1}$. The 2-D model is just an

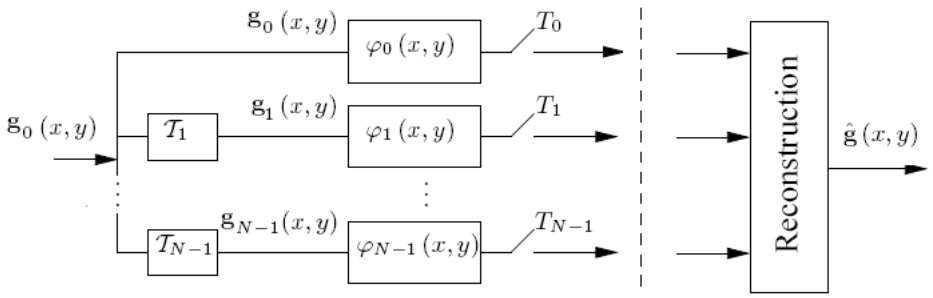

Figure 4.2: **2-D multichannel sampling scenario**

extension to the 1-D case and the only difference is that the delay parameters could be a

combination of more complicated transforms such as scaling, rotation and reflection.

Let us begin by considering the signal $g_0(x, y)$ as the reference signal, and $g_1(x, y)$ as its delayed version where $g_1(x, y) = g_0(x - x_0, y - y_0)$, which is just a translated version of the reference signal. Bearing in mind the formula given in (2.46) for the exponential moments, assume that one parameter is common between the sets $\underline{\alpha}^0$ and $\underline{\alpha}^1$, for example the first and the last parameter of these two sets, i.e. $\alpha_P^0 = \alpha_0^1 = \alpha$. Leaving β_n intact, the exponential moments of the two sampled signals at the corresponding parameters are:

$$\tau_{P,n}^0 = \int_{-\infty}^{\infty}\int_{-\infty}^{\infty} g(x, y)\, e^{\alpha x} e^{\beta_n y}\, dx\, dy \tag{4.7}$$

$$\tau_{0,n}^1 = \int_{-\infty}^{\infty}\int_{-\infty}^{\infty} g(x - x_0, y - y_0)\, e^{\alpha x} e^{\beta_n y}\, dx\, dy, \tag{4.8}$$

which with simple rearranging leads to:

$$\frac{\tau_{0,n}^1}{\tau_{P,n}^0} = e^{\alpha x_0}\, e^{\beta_n y_0}. \tag{4.9}$$

By taking logarithms on both sides we will obtain a system of simple linear equations which we can solve for x_0 and y_0 using matrix equations:

$$\ln\left(\frac{\tau_{0,n}^1}{\tau_{P,n}^0}\right) = \alpha x_0 \; + \beta_n y_0, \tag{4.10}$$

and using matrix equations we can find the shift parameters x_0 and y_0, that is:

$$B^\dagger A = \begin{pmatrix} x_0 \\ y_0 \end{pmatrix},$$

where

$$A = \begin{pmatrix} \ln(\frac{\tau_{0,0}^1}{\tau_{P,0}^0}) \\ \ln(\frac{\tau_{0,1}^1}{\tau_{P,1}^0}) \end{pmatrix} \quad \text{and} \quad B = \begin{pmatrix} \alpha & \beta_0 \\ \alpha & \beta_1 \end{pmatrix}.$$

Therefore if one of the sets of the parameters are common between the two acquisition devices then not only we can exactly retrieve the shifts x_0 and y_0 but also we can easily produce the rest of the exponential moments of both signals all together. This means that, by estimating the shifts, we can produce the higher order moments of the reference signal from the lower order moments of its translated version and vice versa. Finally, by retrieving all the exponential moments, we can use the corresponding reconstruction algorithms to perfectly reconstruct the input 2-D signal. It is important to mention that, in the case of having more than two sensors, we can just set one of the parameters of β_n to be common between the two sets.

As an example for the 2-D Diracs case, assume that we have a multichannel system with 4 E-spline filters, where the reference signal consists of 3 Diracs in a frame size of 256×256,

and the delayed signals are a 2-D translated version of the reference signal. If we want to reconstruct each signal independently, as was shown in Chapter III, a minimum 2-D spline order of $[M, N] = [2K-1, 2K-1] = [5, 5]$ is required for each signal. That is, all the exponential moments $\tau^i_{0:5,0:5}$ are required for an independent perfect reconstruction, but since we can sample the signals symmetrically, the spline orders needed for each image can be reduced. Figure 4.3 illustrates an example of this scenario where α_2 and β_2 are chosen to be common between the sets: $(\underline{\alpha}^0, \underline{\alpha}^1)$ and $(\underline{\beta}^0, \underline{\beta}^1)$. Thus, the following exponential moments are obtained from all the 4 filters: $\tau^0_{0:2,0:2}$, $\tau^1_{2:5,0:2}$, $\tau^2_{0:2,2:5}$ and $\tau^3_{2:5,2:5}$. In the figure, the reference image and its translated versions, their 16×16 under-sampled images with shifts $[x_0, y_0] : [0, 0]; [50, 10]; [50, 50]; [20, 50]$ and spline orders $[M, N] = [2, 2]; [3, 2]; [2, 3]; [3, 3]$, and the reconstructed reference image are all shown. Other images from other sensors could also be reconstructed but only the reconstructed reference image is shown in the figure.

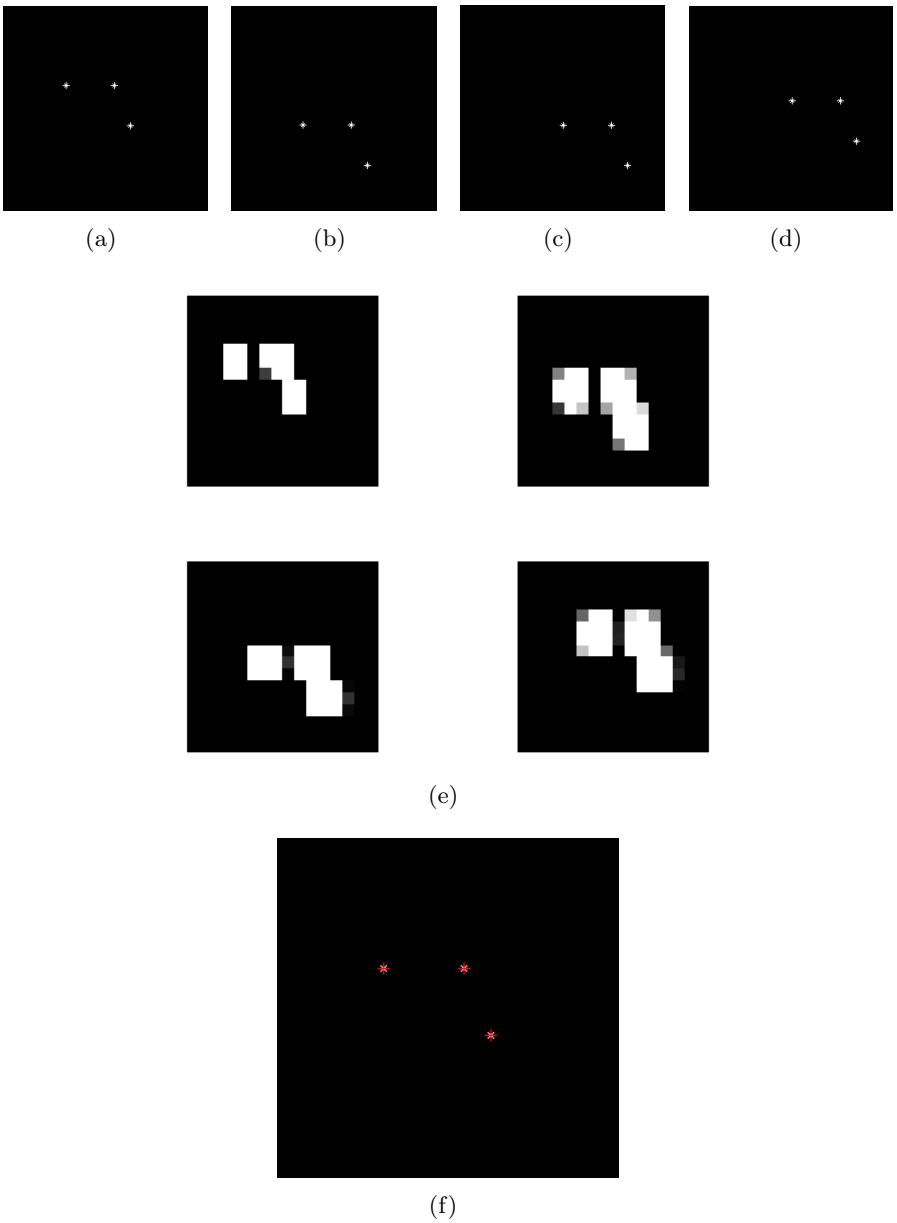

Figure 4.3: **Symmetric multichannel sampling of 2-D Diracs using E-splines (a)(b)(c) & (d) The reference image with $\mathbf{K = 3}$ Diracs in a frame size of $\mathbf{256 \times 256}$ (most-left) and its translated versions (e) The $\mathbf{16 \times 16}$ samples of the reference image (top-left) and the 16 x 16 samples of all other translated images with shifts $[\mathbf{x_0}, \mathbf{y_0}] = [\mathbf{50}, \mathbf{10}]; [\mathbf{70}, \mathbf{70}]; [\mathbf{20}, \mathbf{70}]$ (f) The reconstructed image, the crosses are the retrieved positions of the Diracs. [Not to scale]**

Multichannel sampling of bilevel polygons with only simple translation as the delay parameter, is no different to the case of multichannel sampling of 2-D Diracs. As in the previous case, by setting the common parameters between the $\underline{\alpha}$ sets of the sensors and also the $\underline{\beta}$ sets (in the case of having more than two sensors), the shift parameters x_0 and y_0 can be found by taking logarithms on the exponential moments of both signals. The only difference, which was explained in Chapter III, is the reconstruction algorithm used

for recovering the vertices of the polygon, which in turn changes the minimum spline order required to achieve perfect reconstruction.

As an example, assume again that we have a multichannel system with 4 E-spline filters, where the reference signal is a bilevel triangle in a frame size of 256×256, and the delayed signals are a 2-D translated versions of the reference image. If we want to reconstruct each image independently, as was shown in Chapter III, a 2-D spline order of $[M, N] = [8, 8]$ is required for each image, that is all the exponential moments $\tau^i_{0:8,0:8}$ are required, but since we can sample the images symmetrically, the spline order needed for each image can be reduced. Figure 4.4 illustrates an example of this scenario where α_3 and β_3 are chosen to be common between the sets: $(\underline{\alpha}^0, \underline{\alpha}^1)$ and $(\underline{\beta}^0, \underline{\beta}^1)$. Moreover, the following exponential moments are obtained from all the 4 filters: $\tau^0_{0:3,0:3}$, $\tau^1_{3:8,0:3}$, $\tau^2_{0:3,3:8}$ and $\tau^3_{3:8,3:8}$. In the figure, the reference image and its translated versions, its 16×16 under-sampled image with an spline order of $[M, N] = [3, 3]$, the 16×16 samples of all the other under-sampled images with shifts $[x_0, y_0] : [50, 10]; [70, 70]; [20, 70]$ and spline orders $[M, N] = [5, 3]; [3, 5]; [5, 5]$ and the reconstructed reference image are all shown.

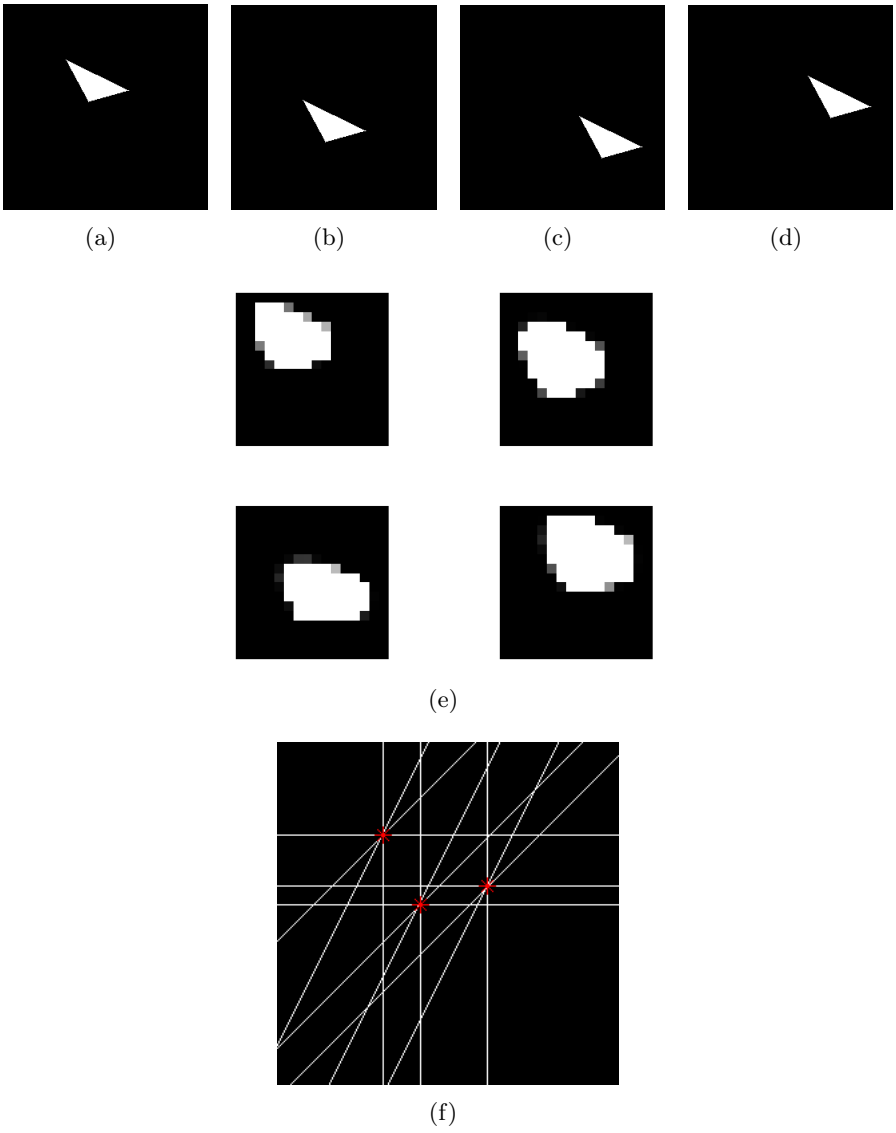

Figure 4.4: **Symmetric multichannel sampling of bilevel polygons using E-splines (a)(b)(c) & (d) The reference bilevel polygon image with $\mathbf{K = 3}$ in a frame size of $\mathbf{256 \times 256}$ (most-left) and its translated versions (e) The $\mathbf{16 \times 16}$ samples of the reference image (most-left) and the $\mathbf{16 \times 16}$ samples of all other translated images with shifts $\mathbf{[x_0, y_0] = [50, 10]; [70, 70]; [20, 70]}$ (c) The reconstructed vertices with $\mathbf{3 + 1 = 4}$ back-projections, the crosses are the actual vertices of the polygon. [Not to scale]**

Chapter 5

Future Research

There are many interesting while challenging open problems to look at in our research area and our aim in this chapter is to give a brief description on what we are going to do next and how our future research is planned:

5.1 Sampling Bilevel Polygons

We showed that by using the projection-slice theorem, we can recover the vertices of bilevel polygons using exponential splines. Since for perfect reconstruction $N + 1$ projections are needed for an N-sided bilevel polygon, the order of E-spline used is $\mathcal{O}(N^2)$ which is quite redundant when compared to the degrees of freedom of the signal $\mathcal{O}(2N)$. One idea would be to try to apply a modified version of the ACMP algorithm to the Fourier transform representation of bilevel polygons and try to solve for the locations of the vertices of the polygon without the need for Radon projections. This is open problem in our research and we will focus mainly on this issue in the next coming months.

5.2 Sampling Under Noisy Conditions

So far, in our research, we have assumed that the measurements are noiseless. In practice this is never true, and we want to see how our sampling schemes perform under noisy channels and also to see if, by increasing the spline order, our reconstruction algorithm would result in better estimations than the case with minimum spline order needed. Our aim is to derive Cramér-Rao (C-R) bounds under noisy conditions, assuming that the noise is white Gaussian with zero mean. We are planning to focus on the topic over next coming year as we also want to look at the multichannel sampling scenario under noisy conditions.

5.3 Multichannel Sampling of Bilevel Polygons

In Chapter 5, we illustrated how we can sample bilevel polygons in a multichannel scenario, with the delay parameters being just a simple translation. In practice, this is usually

not the case, and we want to look at the cases of more complicated delay parameters, such as translation, rotation and scaling. Under our current results for sampling bilevel polygons, we need to use Radon projections in order to estimate the more complicated delay parameters, as, unlike the case of having simple translation only, applying rotation and/or scaling for example, would result in a non-linear relationship between the exponential moments of the signals from the different sensors. Therefore, we can not easily estimate the delay parameters like the way it was done for the simple translation case. This is an open problem in our research and we have come up with some ideas but they are at their early stages of our research. Ideas such as:

a) The projection angle ϕ of a rotated signal with respect to its reference image with an angle θ, is the same projection on the reference image at the angle $\phi + \theta$, therefore if the rotation parameter in known then we can easily separate the $N+1$ projections needed between the different sensors.

b) The scaling parameter, independent of all other mentioned parameters, could easily be found by comparing the zero-th order exponential moments of both signals, as the zero-th order moment equals to the area of the bilevel polygon.

Using these ideas, one has to realize that if all the unknown delay parameters are known and calculated, then the $N+1$ projections needed could easily be separated between the different sensors, in order to sample and perfectly reconstruct the reference image (or other images) in a symmetric manner. Therefore the main problem is to see how we can estimate the delay parameters from either the exponential moments or from the Radon projections. As this is in our main research plan, we will focus mainly on this problem over the next coming year.

5.4 Applications

As we mentioned before, multichannel sampling of signals is used in many modern applications and our aim is to see if E-spline sampling kernels have the potential to be used in such applications. By deriving C-R bounds under noisy conditions and introducing sampling theorems for more complicated transformation parameters, we will be able to utilize our results for E-spline sampling kernels in applications such as image super-resolution [23, 24, 25] and interleaved A/D converters. That is, instead of using one, expensive acquisition device working at very high sampling rates, we can synchronize multiple but cheap acquisition devices working at lower sampling rates and still achieve the same performance. We are planning to look at the application side of our research starting from the third year.

Appendix

Subspace Harmonic Retrieval Algorithms on Different Data Models

In Chapter III we showed that, with the standard data model for harmonic retrieval algorithms we can easily find the poles and also the amplitudes from the signal data points using the ACMP method. The question here is that, if we change the data model would the ACMP method still work to retrieve the poles and the amplitudes? First, we will consider the one dimensional case:

The One Dimensional Case

Let us assume that our data model for the one dimensional case is as follows:

$$I_n = \sum_{i=1}^{D} (\alpha n + \beta)\, a_i \varphi_i^n, \tag{5.1}$$

where the parameters a_i, φ_i, α and β are unknown. With this data model, the 1-D subspace harmonic approach, explained previously, would not be able to retrieve the poles and the amplitudes. Therefore we need to modify the method in order for it to work with the mentioned data model. We propose the following modifications: As before, the data points are arranged into Hankel matrix of size $L \times M$ but this time, because of the parameters n in $(\alpha n + \beta)$, we must have $L \geq 2D + 1$ and $M \geq 2D$. The Hankel matrix H can be decomposed as $H = S.A.T^T$ where matrices S, T and A have the following structures respectively:

$$S = \begin{pmatrix} \beta & \beta & \dots & \beta & \varphi_1 & \varphi_2 & \dots & \varphi_D \\ (\alpha+\beta)\varphi_1 & (\alpha+\beta)\varphi_2 & \dots & (\alpha+\beta)\varphi_D & \varphi_1^2 & \varphi_2^2 & \dots & \varphi_D^2 \\ (2\alpha+\beta)\varphi_1^2 & (2\alpha+\beta)\varphi_2^2 & \dots & (2\alpha+\beta)\varphi_D^2 & \varphi_1^3 & \varphi_2^3 & \dots & \varphi_D^3 \\ \vdots & \vdots & \dots & \vdots & \vdots & \vdots & \dots & \vdots \\ ((L-1)\alpha+\beta)\varphi_1^{L-1} & ((L-1)\alpha+\beta)\varphi_2^{L-1} & \dots & ((L-1)\alpha+\beta)\varphi_D^{L-1} & \varphi_1^L & \varphi_2^L & \dots & \varphi_D^L \end{pmatrix}$$

$$T = \begin{pmatrix} 1 & 1 & \dots & 1 & 0 & 0 & \dots & 0 \\ \varphi_1 & \varphi_2 & \dots & \varphi_D & \alpha & \alpha & \dots & \alpha \\ \varphi_1^2 & \varphi_2^2 & \dots & \varphi_D^2 & 2\alpha\varphi_1 & 2\alpha\varphi_2 & \dots & 2\alpha\varphi_D \\ \vdots & \vdots & \dots & \vdots & \vdots & \vdots & \dots & \vdots \\ \varphi_1^{M-1} & \varphi_2^{M-1} & \dots & \varphi_D^{M-1} & (M-1)\alpha\varphi_1^{M-2} & (M-1)\alpha\varphi_2^{M-2} & \dots & (M-1)\alpha\varphi_D^{M-2} \end{pmatrix}$$

$$A = \begin{pmatrix} a_1 & 0 & \dots & 0 & \dots & \dots & 0 \\ \vdots & \ddots & \vdots & \vdots & \vdots & \vdots & \vdots \\ 0 & \dots & 0 & a_D & 0 & \dots & 0 \\ 0 & \dots & 0 & 0 & a_1 & \dots & 0 \\ \vdots & \vdots & \vdots & \vdots & \vdots & \ddots & \vdots \\ 0 & \dots & \dots & \dots & \dots & 0 & a_D \end{pmatrix}.$$

As can be seen, the matrix S has a generalized Vandermonde structure and when compared to the previous data models, a new block of Vandermonde matrix is added to the matrix. The matrix S therefore satisfies the shift-invariant property, that is: $\overline{S} = \underline{S}\Phi$ where

$$\Phi = \begin{pmatrix} \varphi_1 & 0 & \dots & 0 & \dots & \dots & 0 & 0 \\ \vdots & \ddots & \vdots & \vdots & \vdots & \vdots & \vdots & \vdots \\ 0 & \dots & 0 & \varphi_D & 0 & \dots & 0 & 0 \\ \alpha & \dots & 0 & 0 & \varphi_1 & \dots & 0 & 0 \\ 0 & \alpha & \dots & 0 & 0 & \varphi_2 & \dots & 0 \\ \vdots & \vdots & \ddots & \vdots & \vdots & \ddots & \vdots & \vdots \\ 0 & \dots & \dots & \alpha & \dots & 0 & 0 & \varphi_D \end{pmatrix}.$$

Like before, we take the SVD of the Hankel matrix H and truncate that to H_{2D}:

$$H_{2D} = U_{2D} \times \Sigma_{2D} \times V_{2D}. \tag{5.2}$$

U_{2D} and S span the same column space and it follows that: $U_{2D} = S.Q$, where Q is a non-singular matrix. The poles φ_i can be found by taking the EVD of the matrix pencil, constructed as before, and this gives us:

$$eig(\underline{U_{2D}}^{-1}\overline{U_{2D}}) = \Phi. \tag{5.3}$$

Since EVD is applied to the matrix pencil, only the diagonal elements of the matrix Φ are obtained which contains the poles φ_i with multiplicity two. Thus, we have shown with the data model defined above we can still can use the 1-D subspace harmonic approach, but a modified version of it.

Now let us assume that our data model is as follows:

$$I_n = \sum_{i=1}^{D} (\alpha n^2 + \beta n + \gamma)\, a_i \varphi_i^n, \tag{5.4}$$

where the polynomial order of n in $(\alpha n^2 + \beta n + \gamma)$ is $p = 2$ and the parameters a_i, φ_i, α, β and γ are unknown. Like before, the data points are arranged into a Hankel matrix of dimension $L \times M$, but this time, since the polynomial order of n is $p = 2$, we must have: $L \geq 3D + 1$ and $M \geq 3D$. The matrix H can now be decomposed as: $H = S.A.T^T$ where matrices S, T and A have the following structures respectively:

$$S = \begin{pmatrix} \gamma & \dots & \gamma & (\alpha+\beta)\varphi_1 & \dots & (\alpha+\beta)\varphi_D & \varphi_1^2 & \dots & \varphi_D^2 \\ (\alpha+\beta+\gamma)\varphi_1 & \dots & (\alpha+\beta+\gamma)\varphi_D & (3\alpha+\beta)\varphi_1^2 & \dots & (3\alpha+\beta)\varphi_D^2 & \varphi_1^3 & \dots & \varphi_D^3 \\ (4\alpha+2\beta+\gamma)\varphi_1^2 & \dots & (4\alpha+2\beta+\gamma)\varphi_D^2 & (5\alpha+\beta)\varphi_1^3 & \dots & (5\alpha+\beta)\varphi_D^3 & \varphi_1^4 & \dots & \varphi_D^4 \\ \vdots & \dots & \vdots & \vdots & \dots & \vdots & \vdots & \dots & \vdots \\ ((L-1)^2\alpha+(L-1)\beta+\gamma)\varphi_1^{L-1} & \dots & ((L-1)^2\alpha+(L-1)\beta+\gamma)\varphi_D^{L-1} & ((2L-1)\alpha+\beta)\varphi_1^L & \dots & ((2L-1)\alpha+\beta)\varphi_D^L & \varphi_1^{L+1} & \dots & \varphi_D^{L+1} \end{pmatrix}$$

$$T = \begin{pmatrix} 1 & \dots & 1 & 0 & \dots & 0 & 0 & \dots & 0 \\ \varphi_1 & \dots & \varphi_D & 1 & \dots & 1 & 0 & \dots & 0 \\ \varphi_1^2 & \dots & \varphi_D^2 & 2\varphi_1 & \dots & 2\varphi_D & 2\alpha & \dots & 2\alpha \\ \vdots & \dots & \vdots & \vdots & \dots & \vdots & \vdots & \dots & \vdots \\ \varphi_1^{M-1} & \dots & \varphi_D^{M-1} & (M-1)\varphi_1^{M-2} & \dots & (M-1)\varphi_D^{M-2} & ((M-1)^2-(M-1))\alpha\,\varphi_1^{M-3} & \dots & ((M-1)^2-(M-1))\alpha\,\varphi_D^{M-3} \end{pmatrix}$$

$$A = \begin{pmatrix} a_1 & 0 & \dots & \dots & \dots & \dots & \dots & \dots & 0 \\ \vdots & \ddots & \vdots & \vdots & \vdots & \vdots & \vdots & \vdots & \vdots \\ 0 & \dots & a_D & 0 & \dots & \dots & \dots & \dots & 0 \\ 0 & \dots & 0 & a_1 & \dots & \dots & \dots & \dots & 0 \\ \vdots & \vdots & \vdots & \vdots & \ddots & \vdots & \vdots & \vdots & \vdots \\ 0 & \dots & \dots & \dots & \dots & a_D & 0 & \dots & 0 \\ 0 & \dots & \dots & \dots & \dots & 0 & a_1 & \dots & 0 \\ \vdots & \vdots & \vdots & \vdots & \ddots & \vdots & \vdots & \vdots & \vdots \\ 0 & \dots & \dots & \dots & \dots & \dots & \dots & 0 & a_D \end{pmatrix}.$$

As the matrix S has a generalized Vandermonde structure, it satisfies the shift-invariant property, therefore $\overline{S} = \underline{S}\Phi$ where

$$\Phi = \begin{pmatrix} \varphi_1 & 0 & \dots & \dots & \dots & \dots & \dots & \dots & 0 \\ \vdots & \ddots & \vdots & \vdots & \vdots & \vdots & \vdots & \vdots & \vdots \\ 0 & \dots & \varphi_D & 0 & \dots & \dots & \dots & \dots & 0 \\ 1 & 0 & \dots & \varphi_1 & 0 & \dots & \dots & \dots & 0 \\ \vdots & \ddots & \vdots & \vdots & \ddots & \vdots & \vdots & \vdots & \vdots \\ 0 & \dots & 1 & 0 & \dots & \varphi_D & 0 & \dots & 0 \\ 0 & \dots & 0 & 2\alpha & \dots & 0 & \varphi_1 & \dots & 0 \\ \vdots & \vdots & \vdots & \vdots & \ddots & \vdots & \vdots & \ddots & \vdots \\ 0 & \dots & \dots & \dots & \dots & 2\alpha & \dots & 0 & \varphi_D \end{pmatrix}.$$

As before, we take the SVD of the Hankel matrix H and truncate it to H_{3D}:

$$H_{3D} = U_{3D} \times \Sigma_{3D} \times V_{3D}. \tag{5.5}$$

U_{3D} and S span the same column space and it follows that: $U_{3D} = S.Q$, where Q is a non-singular matrix. Now we can construct the matrix pencil from above, and then take EVD to find the poles Φ: $eig(\underline{U_{3D}}^{-1}\overline{U_{3D}}) = \Phi$. Since we are taking the EVD, only the diagonal elements of the matrix Φ are obtained which contains the poles φ_i with multiplicity three. For higher polynomial orders of n, all we need to do is to increase the dimension of the Hankel matrix H accordingly, that is, we must have: $L \geq (p+1)D+1$ and $M \geq (p+1)D$, where p is the maximum degree of the discrete polynomial n^p.

The Two Dimensional Case - The Modified ACMP Approach

For the two dimensional case, let us start by assuming that our general data model is as follows:

$$I_{m,n} = \sum_{i=1}^{D} (\alpha m + \gamma n + \lambda)\, a_i \varphi_i^m \psi_i^n, \tag{5.6}$$

where the parameters a_i, φ_i, φ_i, α, λ and γ are unknown. The polynomial order of n and m are $q = 1$ and $p = 1$ respectively and both are independent of each other. If the size of the matrix $I_{m,n}$ is $M \times N$ where $M \geq 2D+1$ and $N \geq 2D+1$ then $I_{m,n}$ can be decomposed as: $I_{m,n} = S.A'.T^T$ where matrices S, T and A have the following structures

respectively:

$$S = \begin{pmatrix} \lambda & \dots & \lambda & 1 & \dots & 1 \\ (\alpha+\lambda)\varphi_1 & \dots & (\alpha+\lambda)\varphi_D & \varphi_1 & \dots & \varphi_D \\ (2\alpha+\lambda)\varphi_1^2 & \dots & (2\alpha+\lambda)\varphi_D^2 & \varphi_1^2 & \dots & \varphi_D^2 \\ \vdots & \dots & \vdots & \vdots & \dots & \vdots \\ ((M-1)\alpha+\lambda)\varphi_1^{M-1} & \dots & ((M-1)\alpha+\lambda)\varphi_D^{M-1} & \varphi_1^{M-1} & \dots & \varphi_D^{M-1} \end{pmatrix}$$

$$T = \begin{pmatrix} 1 & \dots & 1 & 0 & \dots & 0 \\ \psi_1 & \dots & \psi_D & \gamma\psi_1 & \dots & \gamma\psi_D \\ \psi_1^2 & \dots & \psi_D^2 & 2\gamma\psi_1^2 & \dots & 2\gamma\psi_D^2 \\ \vdots & \dots & \vdots & \vdots & \dots & \vdots \\ \psi_1^{N-1} & \dots & \psi_D^{N-1} & (N-1)\gamma\psi_1^{N-1} & \dots & (N-1)\gamma\psi_D^{N-1} \end{pmatrix}$$

$$A = \begin{pmatrix} a_1 & 0 & \dots & 0 & \dots & \dots & 0 \\ \vdots & \ddots & \vdots & \vdots & \vdots & \vdots & \vdots \\ 0 & \dots & 0 & a_D & 0 & \dots & 0 \\ 0 & \dots & 0 & 0 & a_1 & \dots & 0 \\ \vdots & \vdots & \vdots & \vdots & \vdots & \ddots & \vdots \\ 0 & \dots & \dots & \dots & \dots & 0 & a_D \end{pmatrix}.$$

The matrices S and T have both generalized Vandermonde structures and the matrix A is a diagonal matrix containing all the amplitudes. Therefore, the matrices S and T satisfy the shift-invariant property, that is: $\overline{S} = \underline{S}\Phi$, $\overline{T} = \underline{T}\Psi$ where

$$\Phi = \begin{pmatrix} \varphi_1 & \dots & 0 & 0 & \dots & 0 \\ \vdots & \ddots & \vdots & \vdots & \dots & \vdots \\ 0 & \dots & \varphi_D & 0 & \dots & 0 \\ \alpha\varphi_1 & \dots & 0 & \varphi_1 & \dots & 0 \\ \vdots & \ddots & \vdots & \vdots & \ddots & \vdots \\ 0 & \dots & \alpha\varphi_D & 0 & \dots & \varphi_D \end{pmatrix}$$

$$\Psi = \begin{pmatrix} \psi_1 & \dots & 0 & \gamma\psi_1 & \dots & 0 \\ \vdots & \ddots & \vdots & \vdots & \dots & \vdots \\ 0 & \dots & \psi_D & 0 & \dots & \gamma\psi_D \\ 0 & \dots & 0 & \psi_1 & \dots & 0 \\ \vdots & \ddots & \vdots & \vdots & \ddots & \vdots \\ 0 & \dots & 0 & 0 & \dots & \psi_D \end{pmatrix}.$$

Now we can simply apply the ACMP algorithm to obtain the poles φ_i and ψ_i, except that the size of the enhanced matrix must be $(D+1)(D+1) \times (D+1)(D+1)$ instead of $D(D+1) \times D(D+1)$.

Now let us consider the data model:

$$I_{m,n} = \sum_{i=1}^{D} (\alpha n + \gamma m + \beta mn + \lambda)\, a_i \varphi_i^m \psi_i^n \tag{5.7}$$

where the joint polynomial order of m and n equals to 2, and the parameters a_i, φ_i, ϕ_i, α, β, λ and γ are unknown. The case with this data model is quite different. We have managed to apply subspace retrieval approaches to solve for φ_i and ψ_i separately, but we still have not managed to apply a modified version of the pairing and restoration techniques used in the ACMP method to this data model. It is an open problem and also in our future research work.

Bibliography

[1] M. Vetterli, P. Marziliano and T. Blu, “Sampling Signals with Finite Rate of Innovation”, IEEE Transactions on Signal Processing, vol. 50, p. 1417-1428, June 2002.

[2] P.L. Dragotti, M. Vetterli and T. Blu, “Sampling Moments and Reconstructing Signals of Finite Rate of Innovation: Shannon meets Strang-Fix”, IEEE Transactions on Signal Processing, vol. 55, pp. 1741-1757, May 2007.

[3] M. Unser and T. Blu, “Cardinal Exponential Splines: Part I - Theory and Filtering Algorithms”, IEEE Transactions on Signal Processing, vol. 53, pp. 1425, April 2005.

[4] P. Shukla and P.L. Dragotti, “Sampling Schemes for Multidimensional Signals with Finite Rate of Innovation”, IEEE Transactions on Signal Processing, vol. 55, pp. 3670-3686, July 2007.

[5] I. Maravic and M. Vetterli, “Exact sampling results for some classes of parametric non-bandlimited 2-D signals", IEEE Transactions on Signal Processing, vol.52, no.1, pp. 175-189, January 2004.

[6] S.W. Lee and R. Mittra, “Fourier transform of a polygonal shape function and its application in electromagnetics," IEEE Transactions on Antennas and Propagation, vol.31, no.1, pp. 99-103, January 1983.

[7] F. Vanpoucke, M. Moonen and Y. Berthoumieu, “An Efficient Subspace Algorithm for 2-D Harmonic Retrieval", IEEE International Conference on Acoustics, Speech, and Signal Processing, vol.4, pp. 461-464, April 1994.

[8] S.R. Deans, “The Radon Transform and Some of Its Applications”, Wiley publication, 1983.

[9] P. Milanfar, G.C. Verghese, W.C. Karl and A.S.Willsky, “Reconstructing polygons from moments with connections to array processing", IEEE Transactions on Signal Processing, vol.43, no.2, pp. 432-443, February 1995.

[10] I. Maravic and M. Vetterli, “A sampling theorem for the Radon transform of finite complexity objects", IEEE International Conference on Acoustics, Speech, and Signal Processing, vol.2, pp. 1197-1200, April 2002.

[11] L. Baboulaz, “Feature Extraction for Image Super-resolution using Finite Rate of Innovation Principles”, PhD thesis, Department of Electrical and Electronic Engineering, Imperial College London, 2008.

[12] T. Blu and M. Unser, “Approximation errors for quasi-interpolators and (multi-)wavelet expansions”, Applied and Computational Harmonic Analysis, vol. 6, pp.219-251, March 1999.

[13] P. Shukla and P.L. Dragotti, “Sampling Schemes for Multidimensional Signals with Finite Rate of Innovation”, IEEE Transactions on Signal Processing, vol. 55, pp. 3670-3686, July 2007.

[14] Y. Hua, “Estimating two-dimensional frequencies by matrix enhancement and matrix pencil", IEEE Transactions on Signal Processing, vol.40, no.9, pp. 2267-2280, September 1992.

[15] D.B. Rao and S. Kung, “A state space approach for the 2-D harmonic retrieval problem", IEEE International Conference on Acoustics, Speech, and Signal Processing, vol.9, pp. 174-176, March 1984.

[16] P. J. Davis, “Triangle formulas in the complex plane”, Journal of Mathematics of Computation, vol. 18, pp.569-577, October 1964.

[17] G. T. Herman, “Image Reconstruction from Projections: The Fundamentals of Computerized Tomography”, Academic Press, New York, 1980.

[18] P. Stoica and R. Moses, “Introduction to spectral analysis”, Prentice-Hall, 2000.

[19] R. E. Blahut, “Theory and practice of error control codes”, Addison-Wesley, 1983.

[20] I. Maravic, “Sampling methods for parametric non-parametric signals: extensions and applications”, PhD thesis, Audio Visual Communication Laboratory, Swiss Federal Institute of Technology (EPFL), Lausanne, Switzerland, 2004.

[21] P. Shukla, “Sampling schemes for multidimensional nonbandlimited signals”, PhD thesis, Department of Electrical and Electronic Engineering, Imperial College London, United Kingdom, 2001.

[22] P. Marziliano, “Sampling Innovations”, PhD thesis, Audio Visual Communication Laboratory, Swiss Federal Institute of Technology (EPFL), Lausanne, Switzerland, 2004.

[23] L. Baboulaz and P.L. Dragotti, “Distributed acquisition and image superresolution based on continuous moments from samples”, IEEE International Conference on Image Processing, Atlanta, USA, October 2006.

[24] L. Baboulaz and P.L. Dragotti, “Image Super-Resolution with B-Spline kernels”, 7th IMA International Conference on Mathematics in Signal Processing, Cirencester, UK, December 2006.

[25] L. Baboulaz and P.L. Dragotti, “Local Feature Extraction for Image Super-Resolution”, IEEE International Conference on Image Processing, San Antonio, USA, September 2007.

[26] N. Gehrig and P.L. Dragotti, “Distributed Sampling and Compression of Scenes with Finite Rate of Innovation in Camera Sensor Networks”, Data Compression Conference, Snowbird, USA, March 2006.

[27] Y. Hao, P. Marziliano, M. Vetterli, and T. Blu, “Compression of ECG as signal with finite rate of innovation”, International Conference of the IEEE Engineering in Medicine and Biology Society, Shanghai, China, September 2005.

[28] I. Jovanovic and B. Beferull-Lozano, “Oversampled A/D conversion and errorrate dependence of nonbandlimited signals with finite rate of innovation”, IEEE Transactions on Signal Processing, vol. 54, pp. 2140–2154, June 2006.

[29] M. Unser, “Splines - a perfect fit for signal and image processing”, IEEE Signal Processing Magazine, vol. 16, pp. 22–38, November 1999.

[30] M. Unser, A. Aldroubi and M. Eden, “B-Spline Signal Processing: Part I—Theory", IEEE Transactions on Signal Processing, vol. 41, pp. 821-833, February 1993.

[31] M. Unser, A. Aldroubi and M. Eden, “B-Spline Signal Processing: Part II—Efficient Design and Applications", IEEE Transactions on Signal Processing, vol. 41, pp. 834-848, February 1993.

[32] I. Daubechies, “Ten Lectures on Wavelets”, Society for Industrial and Applied Mathematics, Philadelphia, USA, 1992.

[33] M. Vetterli and J. Kovacevic, “Wavelets and Subband Coding”, Prentice-Hall, 1995.

[34] G. Strang and G.Fix, “A Fourier analysis of the finite element variational method”, In Constructive Aspect of Functional Analysis, pp. 796-830, Rome, Italy, 1971.

[35] I. J. Schoenberg, “Contribution to the problem of approximation of equidistant data by analytic functions”, Quarterly of Applied Mathematics, vol. 4, pp. 45–99 and 112–141, 1946.

[36] M. Unser, “Sampling - 50 Years after Shannon”. IEEE Transactions on Signal Processing, vol. 88, pp. 569–587, April 2000.

[37] R. Roy and T. Kailath, "ESPRIT-estimation of signal parameters via rotational invariance techniques," IEEE International Conference on Acoustics, Speech, and Signal Processing, vol.37, pp. 984-995, July 1989.

[38] R. O. Schmidt, “Multiple emitter location and signal parameter estimation," IEEE Transactions on Antennas and Propagation, vol. 34, pp. 276-280, March 1986.

[39] S. Y. Kung, K. S. Arun, and D. V. Bhaskar Rao, “State-space and singular-value decomposition-based approximation methods for the harmonic retrieval problem”, Journal of Optical Society of America, vol. 73, issue 12, pp. 1799-1811, December 1983.

[40] B.D. Rao and K.S Arun, “Model based processing of signals: a state space approach", IEEE Transactions on Signal Processing, vol 80, pp 283-309, February 1992.